Results in Engineering 20 (2023) 101600

Contents lists available at ScienceDirect

Results in Engineering

journal homepage: www.sciencedirect.com/journal/results-in-engineering

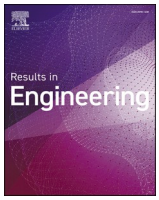

Comparative study of energy performance and water savings between hygroscopic and rankine cycle in a nuclear power plant. Case study of the HTR-10 reactor

Roberto Martínez-Pérez [a], Juan Carlos Ríos-Fernández [a], Guillermo Laine Cuervo [a], Fernando Soto Pérez [a], Francisco J. Rubio-Serrano [b], Antonio J. Gutiérrez-Trashorras [a,*]

[a] Energy Department, Polytechnic School of Engineering, University of Oviedo, Energy Building, Campus of Viesques, 33203, Gijón, Asturias, Spain
[b] IMATECH, IMASA Technologies, S.L.U. St. Carpinteros 12, 28670, Villaviciosa de Odón, Madrid, Spain

ARTICLE INFO

Keywords:
Hygroscopic cycle technology
Regenerative rankine cycle
Cooling water savings
Small modular reactor
Nuclear energy
Energy generation

ABSTRACT

The use of nuclear energy can contribute to achieving positive socio-economic and environmental benefits, but nuclear power plants are one of the most water-intensive industries in the world. The use of Small Modular Reactor (SMR) technologies is increasing due to their interesting advantages such as reduction of construction costs and use in remote areas, which favors distributed generation. Hygroscopic Cycle Technology (HCT) can be of great interest for power generation in nuclear power plants, due to the potential improvement in terms of energy efficiency and water savings. This study presents the benefits of implementing HCT in an existing SMR, the HTR-10, based on the classical Regenerative Rankine Cycle (RRC). The HTR-10 is used to produce electricity and thermal energy for District Heating (DH). Analytical models of both cycles have been developed to compare them in terms of energy production and water consumption. Sensitivity analyses of the influence of the main variables have been performed. The results show that by varying the condensing pressures, the thermal power for DH and the net mechanical power production of the HCT increase up to 2.5 % and 1 %, respectively, with respect to the RRC. The maximum tolerable ambient temperature for the plant with the HCT is 43.12 °C, increasing the availability of the plant and avoiding water consumption between 70000 and 88000 m^3/year, depending on the operating conditions. Extrapolation of the results suggests that HCT can improve the energy production of nuclear power plants in a more sustainable way, contributing significantly to the energy transition.

1. Introduction

The growing concern about climate change and the need to ensure the supply of electricity to a more energy-demanding society, makes it necessary to seek solutions that combine a clean generation (without emissions) with security [1,2]. Renewable energies meet this premise but most of them, have the disadvantage of being intermittent sources that depend on external factors to function (mainly wind and sun), making it difficult to use them efficiently without the use of storage solutions still in development [3–5].

Another technology that fulfills this premise is nuclear energy. According to data from the International Atomic Energy Agency (IAEA), there are currently 441 reactors in operation with a total installed capacity of 393853 MWe, of which 307 are based on the Pressurized Water Reactor (PWR) technology and 61 on the Boiling Water Reactor (BWR) technology. There are also 53 projects under construction which will contribute with 54517 MWe to this total [6,7]. Two of the main problems in the development of these large projects (>1GWe) are the cost overruns and delays during construction, which in some cases can lead to failure [8–10]. However, there is another fact that is becoming increasingly important: water consumption. Thermoelectric generation plants (thermal, combined cycles, nuclear, etc.) need to be close to a water reservoir so the steam generated could be condensed. The amount of water required makes these facilities one of the most water-intensive industries in the world. According to the work of Sesma and Rubio-Varas [11], 80 % of the world's energy production would cease if there were no water. Moreover, their studies have shown that nuclear power plants are the thermoelectric generation technologies that make the greatest use of this resource. In the current context, climate change may exacerbate droughts in various regions of the world, making them more frequent [12] and affecting, not only the aforementioned energy

* Corresponding author.
E-mail address: gutierrezantonio@uniovi.es (A.J. Gutiérrez-Trashorras).

https://doi.org/10.1016/j.rineng.2023.101600
Received 21 August 2023; Received in revised form 5 November 2023; Accepted 15 November 2023
Available online 20 November 2023

Acronyms

4S Super-Safe, Small and Simple Reactor
ABV-6E Afrikantov OKBM
ACPR50S Floating Nuclear Reactor
A-HTR Advanced High Temperature Reactor
AHWR Advanced Heavy-Water Reactor
ALFRED Advanced Lead-cooled Fast Reactor European Demonstrator
ARIS Advanced Reactor Information System
ASTRID Advanced Sodium Technological Reactor for Industrial Demonstration
BWR Boiling Water Reactor
BWRX Boiling Water Reactor tenth evolution
CAREM Modular Elements Argentinian Central
CERMET Ceramic Fuel in a Metal matrix
CFR Compact Fusion Reactor
CLEAR-I China Lead-based Reactor
CO2 Carbon dioxide
DH District Heating
DHR Deep-pool Low-temperature Heating Reactor
DMS Double MS: Modular Simplified & Medium to Small Reactors
EES Engineering Equation Solver
ELECTRA European Lead Cooled Training Reactor
ELFR European Lead Fast Reactor
EM² Energy Multiplier Module
FBNR Fixed Bed Nuclear Reactor
FBR-1 & 2 Fast. Breeder Reactors-1&2
FCM Fully Ceramic Microencapsulated
G4M Gen4Module
GCR Gas Cooled Reactor
GFR Gas Fast Reactor
GTHTR Gas Turbine High Temperature Reactor
HALEU High-Assay LEU
HAPPY Heating-reactor of Advanced low-Pressurized and Passive safetY system
HCT Hygroscopic Cycle Technology
HPW Heavy Pressurize Water
HTMR High Temperature Modular Reactor
HTR High Temperature Reactor
HTR-PM High-Temperature Gas-Cooled Reactor Pebble-Bed Module
HTTR High Temperature Test Reactor
HW Heavy Water
HWR Heavy Water Reactor
IAEA International Atomic Energy Agency
IMR Integrated Modular Water Reactor
INET Institute of Nuclear and New Energy Technology
IPHWR Indian Pressurized Heavy Water Reactor
iPWR Integrated PWR
IRIS International Reactor Innovative and Secure
KP-FHR Kairos Power Fluoride Salt-Cooled High-Temperature Reactor
LBR Lead Bismuth Reactor
LEU Low Enriched Uranium
LFR Lead Fast Reactor
LFR-AS Lead-cooled Fast Reactor Amphora-Shaped
LFR-TL-X Lead-cooled Fast Reactor Transportable reactor and Long-life core
LFTR Liquid Fluoride Thorium Reactor
LW Light water
MBIR Multipurpose Fast-Neutron Research Reactor
MCSFR Molten Chloride Salt Fast Reactor
MHR Modular Helium Reactor
Mk1 PB-FHR Mark-I Pebble-Bed Fluoride-Salt-Cooled, High Temperature Reactor
MMR Micro Modular Reactor
MoveluX Mobile-Very-small reactor for Local Utility in X-mark
MOX Mixed Oxide
MOX Mixed Oxide
MSR Molten Salt Reactor
MSTW Molten Salt Thermal Wasteburner
MYRRHA Multi-purpose Hybrid Research Reactor for High-Tech Applications
PBMR Pebble Bed Modular Reactor
PEACER Proliferation-resistant Environment-friendly Accident-tolerant Continual Economical Reactor
PGSFR Prototype Gen-IV Sodium-cooled Fast Reactor
PHWR Pressurized HWR
Prism Power Reactor Innovative Small Module
PWR Pressurized Water Reactor
RDE Experimental Power Reactor
RRC Regenerative Rankine Cycle
SC-HTGR Steam Cycle High Temperature Gas-Cooled Reactor
SEALER Swedish Advanced Lead Reactor
SFR Sodium Fast Reactor
SmAHTR Small Modular Advanced High Temperature Reactor
SMART System-Integrated Modular Advanced Reactor
SMR Small Modular Reactor
SmTMSR Small Modular Th-based Molten Salt Reactor
SSR - Waster Burner Stable Salt Reactor
SUPERSTAR Enhanced Refined Secure Transportable Autonomous Reactor
SVBR Lead–bismuth Fast Reactor
TRISO Tristructural Isotropic
TRU Transuranic
TWR-P Travelling Wave Reactor-Prototype
UO2 Uranium Oxide
VK Reactor Module Viruskiller
VVER Water-Water Energetic Reactor
VVER Water-Water Energetic Reactor
W-LFR Westinghouse Lead Fast Reactor
W-SMR Westinghouse Small Modular Reactor

production [11], but also food crops [13], livestock [14] and even its direct consumption by humanity, particularly in arid or semi-arid areas [15]. Countries such as the USA, France, India, China, or Brazil, have seen how restrictions on water consumption have affected their production systems [16].

The use of nuclear energy is still viewed with suspicion by some sectors of society [17,18]. However, it is a low-carbon energy source with low direct and indirect CO_2 emissions [19] and it is essential in mitigating environmental pollution, as reflected in the Special Report on Global Warming of 1.5 °C [20] and the earlier Fifth Assessment Report of the Intergovernmental Panel on Climate Change [21]. On the other hand, the current global energy context positions nuclear energy as an alternative to fossil fuels to become a baseload energy source [22]. Therefore, the use of nuclear energy can contribute to achieve positive socio-economic and environmental benefits as it is safer, less sensitive to carbon emissions, and produces less waste than other energy sources such as hydro and wind power [23]. In this context, nuclear energy has started to be considered as a "green energy technology", including as a key player in the achievement of the Sustainable Development Goals set by the UN in 2015 [24]. Accordingly, the European Parliament has

included some activities related to nuclear energy in the list of environmentally sustainable economic activities to which the so-called "EU taxonomy" applies [25]. The Taxonomy Regulation is part of the Commission's Action Plan for financing Sustainable Growth and aims to promote green investment and prevent greenwashing by companies. For example, the Commission believes that private investment in nuclear energy has an important role to play in the environmental transition. It has therefore proposed that certain activities related to nuclear energy be considered as transition activities contributing to the mitigation of climate change [26]. The inclusion of such activities is limited in time and subject to specific requirements under conditions of transparency. Equally important, however, is the low impact of this energy source on relevant aspects such as human health, biodiversity or the responsible use of land, as confirmed, among others, by the studies carried out by Hirschberg et al., in 2016 [27], Cheng and Hammond in 2017 [28] and Brook and Bradshaw in 2014 [29]. These are some of the reasons why the nuclear sector is showing a growing interest in the Small Modular Reactor (SMR) technologies. This type of reactor would include all the advanced reactors capable of producing up to 300 MWe (or even 700 MWe if the Medium Modular Reactors are also included) [30]. The main advantages of these technologies are the reduction of construction costs, flexibility of siting and improvements in safety (safety systems designed to prevent rather than control risks and safety in relation to proliferation) [30–34]. Likewise, they would make it possible to bring electricity to remote areas, favoring distributed generation. They also represent an important advantage in areas affected by natural disasters, where a constant and secure source of energy may be needed. As the power range is relatively wide, a subset of reactors called micro-reactors has been defined with a power below 20 MWe. These reactors could be presented as alternatives to other technologies commonly used to generate heat or electricity in remote or critical areas, such as diesel generators, and have a valuable advantage in that they do not require continuous refueling [33].

It is difficult to estimate how many different SMRs there are, as some of the designs are still in the early stages of development. The 2014 paper by Zhitao Liu and Jihon Fan [35], analyzes the three SMR models they consider to be the most developed: mPower, Westinghouse SMR, and NuScale. In 2015, Rowinski et al. [32] has expanded the previous list to twenty-five models of small and medium modular reactors, classified by technology and coolant used. These reactors are of Generation III/III+ and IV and range in power from 6.5 MWe of the Russian KLT40-S (PWR) to 740 MWe of the Canadian EC6 (Heavy Water Reactor - HWR). In 2015, Testoni et al. [33] conducted a study focusing on micro-reactors and analyzed eight designs in an advanced stage of development: eVinciTM, Aurora, Holos-Generator, Xe-Mobile, NuScale, SEALER, U-Battery and MMRTM. With all this information, a list of thirty-three different SMRs can be made. However, there are several other models (at different stages of development) that could be included in this list, such as those identified by the IAEA in its document "Advances in Small Modular Reactor Technology Development" [36]. The IAEA Department of Nuclear Energy supports the efforts of Member States in the development of Small Modular Reactors (SMRs), considering them as a practical solution for energy security in countries interested in SMRs. Advances in technology and design of SMRs are presented in the publication, including molten salt, marine and land based water-cooled, high temperature gas cooled and the micro modular reactors up to 10 MW. Also, the models available in the in the ARIS website (Advanced Reactor Information System) [37] are considered. Specifically, it includes the most up-to-date data on nuclear power plant design and major development trends, including reactors of all sizes and types, and evolutionary nuclear power plant designs for both near-term deployment and breakthrough reactors under development. According to those sources, a total of ninety-three different models can be considered (Table 1).

The reactors in Table 1 have been grouped by technology. It can be seen that 26 of the 93 models are based on PWR technology and 5 on

Table 1
Small Modular Reactors List [36,37].

Type	Design	Output (MWe)	Coolant	Fuel
BWR	BWRX-300	270–90	LW	UO2
BWR	DMS	300	LW	UO2
BWR	KARAT-100	100	LW	UO2
BWR	KARAT-45	45–50	LW	UO2
BWR	VK-300	250	LW	UO2
GCR	A-HTR-100	50	Helium	LEU
GCR	GTHTR300	100–300	Helium	TRISO
GCR	HTMR-100	35	Helium	TRISO
GCR	HTR-10	2.5	Helium	TRISO
GCR	HTR-PM	210	Helium	UO2
GCR	HTTR-30	30 MW_{th}	Helium	TRISO
GCR	MHR-100	25–87	Helium	Coated LEU
GCR	MHR-T	4 × 205	Helium	Coated LEU
GCR	PBMR	165	Helium	TRISO
GCR	Prismatic HTR	150	Helium	TRISO
GCR	RDE	3	Helium	LEU/Spent
GCR	StarCore	14/20/60	Helium	TRISO
GCR	Xe-100	82.5	Helium	TRISO
GFR	ALLEGRO	75 MW_{th}	Helium	MOX
GFR	EM^2	265	Helium	LEU
GFR	SUPERSTAR	120	Lead	U-Pu-Zr
HWR	AHWR	920 MW_{th}	LW	MOX
HWR	DHR400	400 MW_{th}	LW	UO2
HWR	IPHWR-220	236	HW	UO2
HWR	TEPLATOR	50 MW_{th}	HW	VVER-440
iPWR	IMR	350	LW	LEU
iPWR	NuScale	12 × 60	LW	UO2
iPWR	SMART	100	LW	UO2
iPWR	W-SMR	225	LW	UO2
LBR	microURANUS	20	Pb–Bi Eutectic	UO2
LFR	ALFRED	125	Lead	MOX
LFR	ARC-100	100	Sodium	U–Zr alloy
LFR	BREST-OD-300	300	Lead	PuN - UN
LFR	CLEAR-I	10 MW_{th}	Pb–Bi Eutectic	UO2
LFR	ELECTRA	0.5 MW_{th}	Lead	(Pu, Zr)N
LFR	ELFR	630	Lead	MOX
LFR	G4M	25	Pb–Bi Eutectic	UN
LFR	LFR-AS-200	200	Lead	UO2
LFR	LFR-TL-X	5–20	Lead	LEU
LFR	MYRRHA	100 MW_{th}	Pb–Bi Eutectic	MOX
LFR	PEACER	300	Pb–Bi Eutectic	U-TRU-Zr
LFR	SC-HTGR	272	Helium	TRISO
LFR	SVBR-100	100	Pb–Bi Eutectic	UO2
LFR	W-LFR	450	Lead	UO2/MOX
MSR	FUJI	200	Molten Fluoride	Molten Salts
MSR	Integral MSR	195	Fluoride Salts	Molten Salts
MSR	KP-FHR	140	Li2BeF4	TRISO
MSR	LFTR	250	Fluoride Salts	Thorium
MSR	MCSFR	50–1200	Molten Salt	Molten Salts
MSR	Mk1 PB-FHR	100	Fluoride Salts	TRISO
MSR	MSR-FUJI	200	Fluoride Salts	Molten Salts
MSR	MSTW	115	Molten Salt	Molten Salts
MSR	SEALER	55	Lead	UN
MSR	SmAHTR	125 MW_{th}	Fluoride Salts	TRISO
MSR	smTMSR-400	168	Molten Salt	Molten Salts
MSR	SSR - Waster Burner	300	Molten Salt	Molten Salts
MSR	ThorCon	2 × 250	Molten Salt	Molten Salts
PHWR	CANDU SMR	300	HW	Natural U
PWR	ABV-6E	6–9	LW	UO2
PWR	ACP100	100	LW	UO2
PWR	ACPR50S	50	LW	UO2
PWR	CAP200	200	LW	UO2
PWR	CAREM	30	LW	UO2
PWR	ELENA	68 kW	LW	UO2/MOX
PWR	FBNR	72	LW	CERMET
PWR	HAPPY200	200 MW_{th}	LW	UO2
PWR	IRIS	335	LW	UO2/MOX
PWR	KLT-40S	2 × 35	LW	LEU
PWR	mPower	2 × 195	LW	UO2
PWR	NUWARD	2 × 170	LW	UO2
PWR	RITM-200	2 × 53	LW	UO2
PWR	RUTA-70	70 MW_{th}	LW	CERMET

(*continued on next page*)

Table 1 (*continued*)

Type	Design	Output (MWe)	Coolant	Fuel
PWR	SHELF	6.6	LW	UO2
PWR	SMR-160	160	LW	UO2
PWR	UK-SMR	443	LW	UO2
PWR	UNITHERM	6.6	HPW	UO2
PWR	VBER-300	325	LW	UO2
PWR	VVER-600	600	LW	UO2
PWR	VVER-640	645	LW	UO2
SFR	4S	10	Sodium	U–Zr alloy
SFR	ASTRID	600	Sodium	MOX
SFR	CFR-600	600	Sodium	UO2/MOX
SFR	FBR-1 & 2	500	Sodium	MOX
SFR	MBIR	60	Sodium	MOX
SFR	PGSFR	150	Sodium	U-(TRU)-Zr
SFR	Prism	311	Sodium	U-Pu-Zr
SFR	TWR-P	600	Sodium	U–Zr alloy
SMR	Aurora	1.5	Liquid metal	HALEU
SMR	Energy Well	8	Fluoride Salts	TRISO
SMR	eVinci	2–3.5	Heat pipes	TRISO
SMR	MMR	5–10	Helium	FCM
SMR	MoveluX	3–4	Sodium	Silicide
SMR	U-Battery	4	He - N	TRISO

BWR technology, i.e. about 1/3 of the designs considered correspond to or are based on the most widely used light water reactor technologies. This makes sense, as these are proven technologies. However, it can also be seen that there are a significant number of gas-cooled fast reactors (GCR and GFR) and metal-cooled (lead - LFR; and sodium - SFR). These reactors lack a moderator and therefore cannot be cooled with water (light or heavy). The predominant form of fuel is UO2, generally in the form of pellets, although TRISO is presented as the most suitable fuel for GCR and MOX for SFR. On the other hand, Generation IV MSRs use a mixture of molten salts as coolant and fuel. Most SMRs are designed to produce electricity in combination with some co-generation technology such as district heating, water desalination [38], hydrogen production [39] or synthetic fuels [40]. However, models such as the DHR400, Happy 200, TEPLATOR, RUTA-70 or ELENA have been designed for district heating only [41].

Electricity generation by nuclear reactors, whatever their type (large, medium, small or micro), requires a turbine that works with the steam generated in a steam generator in which the reactor coolant (water, gas, liquid metal, molten salts, etc.) comes into contact with the water of the steam cycle. The most common working cycle used in steam cycles is the Rankine Cycle (RC) [42,43]. In this cycle, mechanical work from steam expansion at a turbine is transferred to a generator to deliver electrical power [44]. Over the years, improvements have been made to this thermodynamic cycle in order to increase the conversion efficiency [45]. Some of the ways to achieve this are supercritical cycles, overheating or regenerative cycles (a modification of the thermodynamic parameters), but also by improving the quality of the fuels, their composition, the materials used and even the turbine design [46–50]. Thus, the performances obtained nowadays are between 34 and 36 % [51]. In more detail, improvements that have been introduced throughout history to increase the efficiency of the RC are not only limited to equipment upgrades (such as pumps, turbine, and boiler), but also to modifications in the plant layout. Major improvement efforts to date mainly consist of modification of operating conditions, such as steam superheating (Hirn cycle) [52], increase of boiler pressure or decrease of expansion pressure [53]. Other options are reheating processes or regenerative feedwater heaters. Reheating processes throughout turbine expansion [54] allow to increase cycle efficiency and reduce humidity at the end of the expansion [55], whereas regenerative feedwater heaters use steam extractions from the turbine to preheat the boiler feedwater [56]. Finally, two different circuits at different operating conditions may be combined in series (binary cycle) to increase global efficiency [57]. Current research trends introduce different working fluids for improving the thermal efficiency of power cycles. For instance, Organic Rankine Cycles (ORCs) operate with organic fluids [58,59] to extract heat from low temperature sources [60] while reaching competitive efficiency levels [61]. ORCs are also used for waste heat harvesting [62] and trigeneration systems [63]. The main disadvantages of traditional RC compared with OCR were published in Refs. [64,65]. The most important disadvantages of RC versus OCR are that RC is less efficient at low temperatures, the isentropic efficiencies of the turbines are lower, smaller evaporator pinch point, greater risk of droplet erosion in the expansion because of excessive humidity, water analysis is mandatory, less compact and more expensive equipment, possible corrosion, and higher velocity of steam leakages. Regarding the disadvantages and of RC in nuclear power plants, most of them use water, e.g. light water reactors (LWR) and, others separate the water-steam circuit from the main coolant circuit, thus avoiding turbining contaminated steam. However, in a BWR (a type of LWR) steam is generated directly in the core and turbined. This makes it necessary for the turbine to have some shielding. The working pressures and temperatures of the main coolant are different. The first one generates steam in a heat exchanger and the second one, directly in the core vessel [66].

Fig. 1 shows the most common schemes of a standard Regenerative Rankine Cycle (RRC) for a non-nuclear power plant (Fig. 1a) and nuclear power plant (Fig. 1b). According to those schemes the difference between them is that in the non-nuclear plant the live steam is generated in a boiler, while in the nuclear plant the live steam is generated in a heat exchanger (steam generator). It is necessary an extra circuit with a coolant that extracts the heat from the nuclear reactor. That heat is used to produce the live steam in the steam generator, but it is a closed heat exchanger to avoid the contamination of the steam (the coolant and the steam are not mixed). Consequently, the RRC is used in nuclear power plants considering the steam generator instead of the boiler.

The power cycles mentioned face several challenges, mainly due to atmospheric and geographical conditions. High ambient temperatures significantly reduce the cooling capacity of the refrigeration systems [67]. Furthermore, for open-loop refrigeration systems the availability of an endless and ensured source of water located near the power plants is fundamental. Power generation accounts for about 10 % of worldwide water consumption, mostly as cooling water [68]. Dry weather conditions intrinsic to many locations in the world, as well as the increasing likelihood of water shortages due to climate change, represent an important aspect relative to the performance of power plants. In RC, once the steam leaves the turbine, it must be condensed to return it to the cycle, consuming significant amounts of water. The amount of water required may vary depending on the technology used to condense the steam. It must be considered that water may also be required to cool some of the equipment present in the plant. Water consumption is defined as the difference between the amount of water withdrawn from the reservoir and the amount returned after steam condensation. According to the 2012 results of Macknick et al. [69], the technology with the highest water consumption is the one that uses cooling towers to condense the steam, with an average of 2.54 m^3 per MWh produced. On the other hand, the use of an open cycle requires a significant amount of water withdrawal (Table 2). Both technologies can cause serious problems in the event of drought: on the one hand, the consumption of the cooling towers could be excessive and, on the other hand, the withdrawal of the amount of water required by the open circuit could leave a river with a flow below-the-ecological level.

In Fig. 2, a scheme of an open-loop counterflow cooling tower is shown. In those cooling towers, air and water come into direct contact to lower the temperature of the hot water. In the process, small amounts of water are evaporated, lowering the water temperature as it moves down in the tower. A distribution system uses multiple nozzles to spray the hot water onto the fill media. This slows the water flow and increases the surface area of the water in contact with the air to enhance the heat transfer process between them. The air is drawn up by a fan so that it passes through the tower in the opposite direction of the water flow.

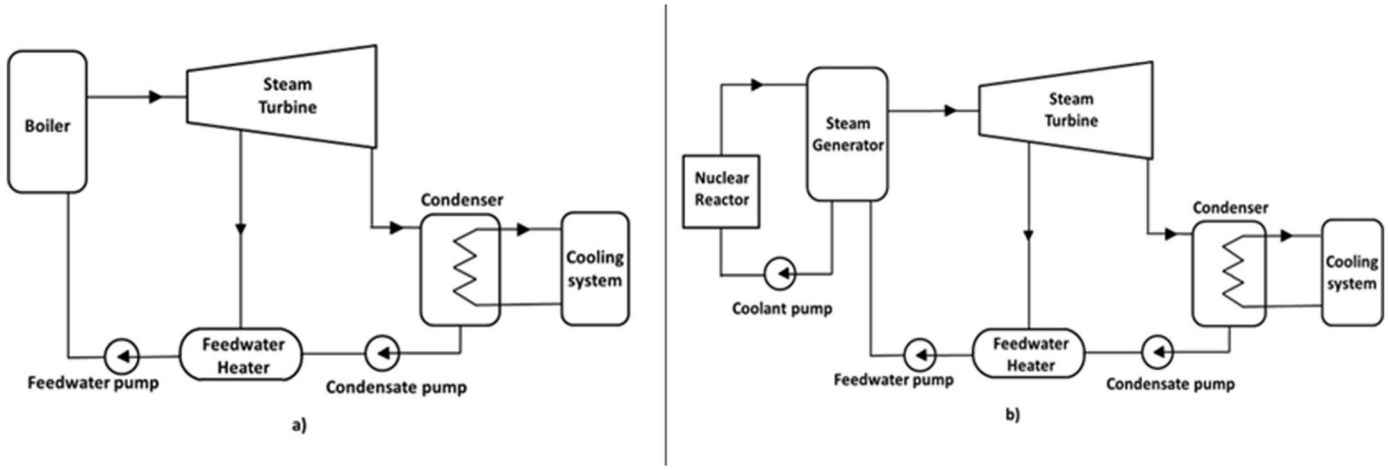

Fig. 1. Scheme of regenerative Rankine cycle: a) non-nuclear power plant, b) nuclear power plant.

Table 2
Water withdrawal and consumption according to technology used [11,69].

	Water withdrawal factor (m^3/MWh)			Water consumption factor (m^3/MWh)		
Cooling Technology	Min	Max	Median	Min	Max	Median
Cooling towers	3.03	9.84	4.17	2.20	3.20	2.54
Open loop	94.64	227.12	167.88	0.38	1.02	1.51

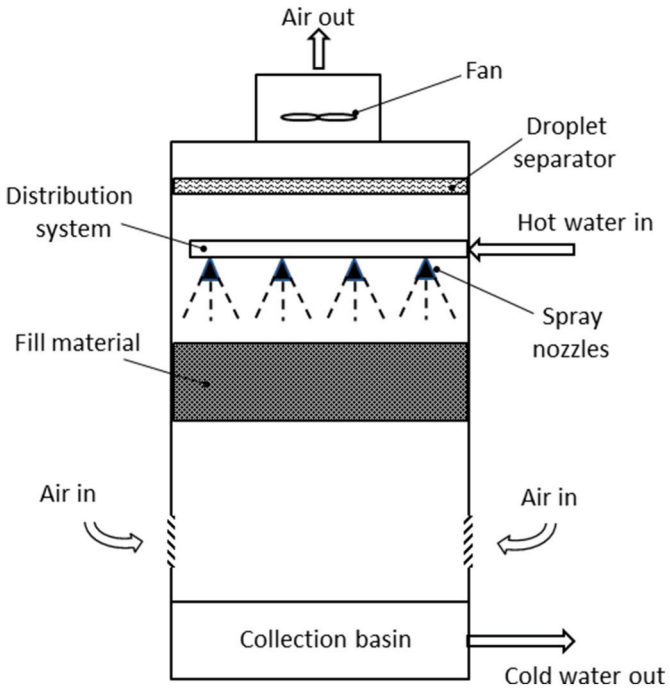

Fig. 2. Scheme of a cooling tower.

Water is collected in the collection basin and exits the tower as cold water, while the air exits warmer and more humid than at the air inlet. In addition, a droplet separator is located at the top of the tower to retain most of the water droplets than are dragged by the air stream, reducing the losses of water [70].

In [71], the authors expand the previous works available in the literature on water consumption for energy production by considering the geographic distribution of water use. They define and calculate an indicator to compare the water consumption of energy production in more than 150 countries. They conclude that about 52 billion m3 of water per year is consumed for global energy production. According to Ref. [72], the use of efficient water-saving cooling technologies is vital. Currently, in thermal power plants, dry cooling and evaporative wet cooling are progressively replacing water-intensive, once-through wet cooling. The authors propose the use of radiative stand-alone cooling systems. With that systems, it is possible to reach 100 % water cooling savings.

Recently, Rubio-Serrano et al. [73] have developed a technology that not only improves the efficiency of the Rankine cycle, but also eliminates the need for cooling water for the steam condensation. This fact makes it ideal for its use and application in remote areas or with water scarcity. This technology is called Hygroscopic Cycle Technology (HCT) and it is characterized by the use of hygroscopic compounds that optimize condensation at the turbine outlet in a condensation chamber [74]. HCT is considered as an alternative to RC towards more sustainable and environmentally friendly technologies [75]. Although this technology can potentially be applied to any generation range, it is currently working in small power plants, such as the 12.5 MW_e "Vetejar" and the 25 MW_e "Agroenergética de Baena" olive biomass plants, both located in the province of Córdoba (Spain). In both cases, the results were positive. In Vetejar, for example, the following results were obtained [76]:

- Reduction of electrical consumption of air coolers used to condense steam by 35 %.
- Water consumption for steam condensation was reduced to zero, saving 229000 m^3 of raw water per year. This is particularly important in Cordoba, where summer temperatures are very high and water restrictions are common.
- Improvement of the plant availability. Prior to the installation of the HCT, the plant had difficulty condensing the steam when the ambient temperature rose above 35 °C. In such situations, the plant had to stop producing energy. With the HCT, this problem disappeared, and the plant operated at full load up to 45 °C.
- Increase the overall plant performance by 2.5 %.

Experimental studies on the HCT performance have been developed by Rubio-Serra et al. in a pilot plant that reproduces all the processes of the cycle. The influence of cooling temperature in the cooling system of the HCT was presented in Ref. [77]. The increase of the saline concentration of the working fluid significantly increases the cooling temperatures, reducing the electrical power consumed by the refrigeration system, and avoiding the water consumption of the cooling towers necessary in many existing power plants. The detailed study of saline concentration in HCT was presented in Ref. [74]. When the

concentration of the hygroscopic salt (lithium bromide in this study) is rose, the power output increases with reference to RC, considering the same condensing temperature in both cycles. The electrical efficiency can reach values over 2.6 % for concentrations of salts higher than 45 %. Also, the effect of the electrical conductivity of the working fluid was experimentally studied in Ref. [78]. Decrease in electrical conductivities in the HCT stabilized at a boiler blowdown ratio (mass flow rate of boiler blowdowns/mass flow rate of the boiler feedwater) of 5 %. Ratios over 10 % did not significantly lower the boiler Cycles of Concentration compared with the increase of pumping power and energy losses.

Analytical studies on the performance of HCT have been published in different papers. In Ref. [79], an exergy analysis of the HCT and RC was presented. The results show that exergy efficiency of the HCT can be 2.52 % higher than for RC at elevated cooling temperatures. Waste heat produced in the HCT with high concentrations of lithium bromide was studied in Ref. [80] for energy use. In that paper, it was used for the waste heat of biomass fuels from olive oil production. An analytical model of the cooling system in the Hygroscopic Cycle power plant was presented in Ref. [81]. The model allows designing specific equipment to fulfil the needs of the cooling system of the HCT [82]. developed an analytical study of the absorber performance of the HCT for low concentrations of the working fluid. According to the results, the thermodynamic properties of the working fluid with concentrations lower than 0.01 % can be approximated to those of pure water. For concentrations ranging in the interval from 0.01 to 5 % the specific enthalpy of the condensate decreases, and both the specific energy dissipated at the dry-coolers and the consumption of the cooling system is lowered. However, according to the results obtained in the pilot plant of the HCT, the efficiency of the cycle in the interval mentioned is not substantially enhanced compared to the one obtained when working with concentrations lower than 0.01 %.

The improvement in efficiency of the HCT respect to RC is interesting, but what is more remarkable is the significant reduction in water consumption. This allows the plant to operate under conditions where it could not with RC, such as in the summer when high temperatures combine with a lack of water due to low rainfall. In Ref. [83] cooling water savings were calculated assuming the implementation of HCT to actual thermoelectric power plants in the Canary Islands. Over 20 different power plants were considered in this study. The cooling systems of those plants were potentially changed by dry coolers by means of the installation of the HCT instead of the RC. The existing cooling systems in those power plants are close cycle desalinated water, open cycle sea water and adiabatic cooling: each of them has different water ratio consumption with an average of 0.38 m^3/MWh. Savings achieved in the power plants located in the Canary Islands accounts for 1.6 Mm^3/year. This result highlights the interest of the use of HCT in power plants for reducing water consumption. Note that, according to Fig. 1, the RRC, and therefore, the HCT can be used in a nuclear plant in which the boiler is replace by a steam generator.

Currently, there are no articles in the scientific literature regarding the application of HCT in nuclear power plants and the extent to which water consumption is optimized with this technology. Therefore, the objective of this paper is to analyze the impact of the HCT technology in an SMR to quantify how the water consumption is reduced, thus making it more viable in remote or critical areas. To this end, the implementation of HCT in an existing nuclear reactor is studied under different operating conditions to analyze its potential benefits in terms of energy production and cooling water savings. The actual HTR-10 nuclear reactor was selected, which operates with a RRC for both electrical power and thermal power for district heating production. Analytical models of both the RRC and the HCT operating at industrial scale conditions (with hygroscopic compounds concentration lower than 0.01 %) were developed to analyze the advantages of implementing the HCT in the nuclear power plant. In addition, a comparison between the energy performance of the HCT and that of the RRC is presented. Also, the consumption of cooling water in the cooling tower of the RRC that can be avoided by implementing the HCT has been studied. Finally, sensitivity analyses of the main parameters such as condensing pressure, bleeding mass flow rate, ambient temperature and ambient relative humidity have been addressed. EES software has been used to perform the analysis.

2. Methodology

Fig. 3 presents a flowchart of the methodology followed in this paper. After the reactor selection according to some criteria defined bellow, the analytical models of both RRC and HCT are developed by applying mass and energy conservation principles to the equipment of the two layouts. Input and output variables of the models are also indicated in the flowchart. The models are validated with the experimental data provided by the pilot plant. Base cases of RRC and HCT are defined for the comparison of the cycles and as a reference for the further sensitivity analyses performed. The variables used for those analyses are indicated in the flowchart.

2.1. Selection of the reactor

The method for selecting a specific reactor in this study is based on the following set of characteristics:

1) Designed for power generation.
2) Low power, since HCT is currently applied to small power ranges (less than 25 MWe).
3) In operation for more than 10 years, in order to have data from a reliable and contrasted installations.
4) With a boiler or steam generator that allows the desorption of the hygroscopic compounds in a drum from which the blowdowns can be extracted, providing a continuous stream (not intermittent).
5) With available thermodynamic data of the whole cycle.

Consequently, all SMRs above 25 MWe in Table 1 have been excluded. Reactors designed for specific solutions such as district heating [41] are also excluded. Finally, the current state of development of the reactors (Table 1) is considered [36,37]. With these considerations in mind, the model finally selected was the HTR-10, built at the Institute of Nuclear and New Energy Technology (INET) of Tsinghua University in China, since it meets all the conditions sought and has been operating at full power since 2003 [84]. Detailed data on the cycle are also available in the literature [85]. It is a high-temperature gas-cooled reactor capable of producing 10 MW_{th}, using helium as coolant and graphite as moderator. The fuel consists of TRISO particles with 17 % enriched uranium arranged in a pebble bed in the reactor core [84]. The helium flows through the reactor core from top to bottom, collecting the heat generated by the fuel and transferring it to the steam generator located in an attached vessel. Here, the heat is transferred to the steam cycle and the helium returns to the core. Analytical models of HTR-10 with Regenerative Rankine Cycle (RRC) and cooling tower and HTR-10 with HCT were developed to perform the analysis. EES software was used to implement the mathematical models of both RRC and HCT [86]. EES is a program that can numerically solve nonlinear algebraic and differential equations and has a database of thermodynamic and transport properties for hundreds of substances, which allows it to be used in studies such as this.

2.2. Analytical models

Current thermodynamic cycle used in the actual HTR-10 is based in the RRC according to Fig. 4. The cycle uses a steam generator to provide the steam at high temperature and pressure (1). It is a cogeneration plant to produce both electrical power in the turbine and thermal power for a District Heating (DH) system. There is a steam extraction (2) in the turbine for the DH and further connection (6) to the Deaerator that also

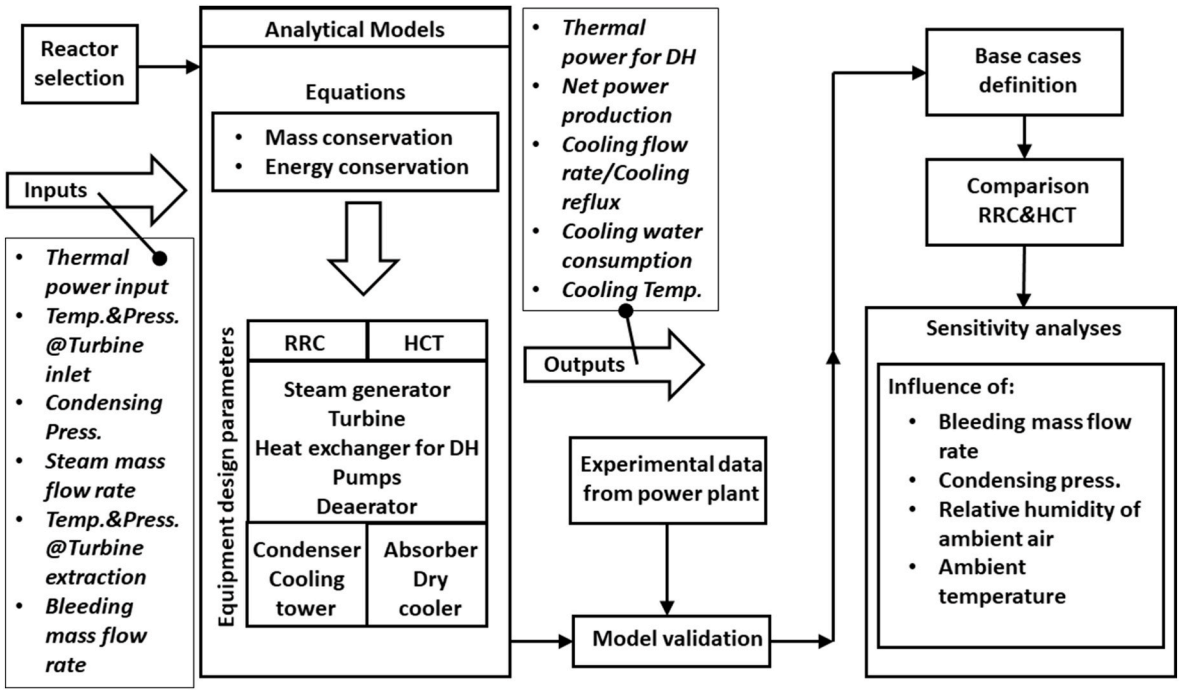

Fig. 3. Flowchart of the methodology.

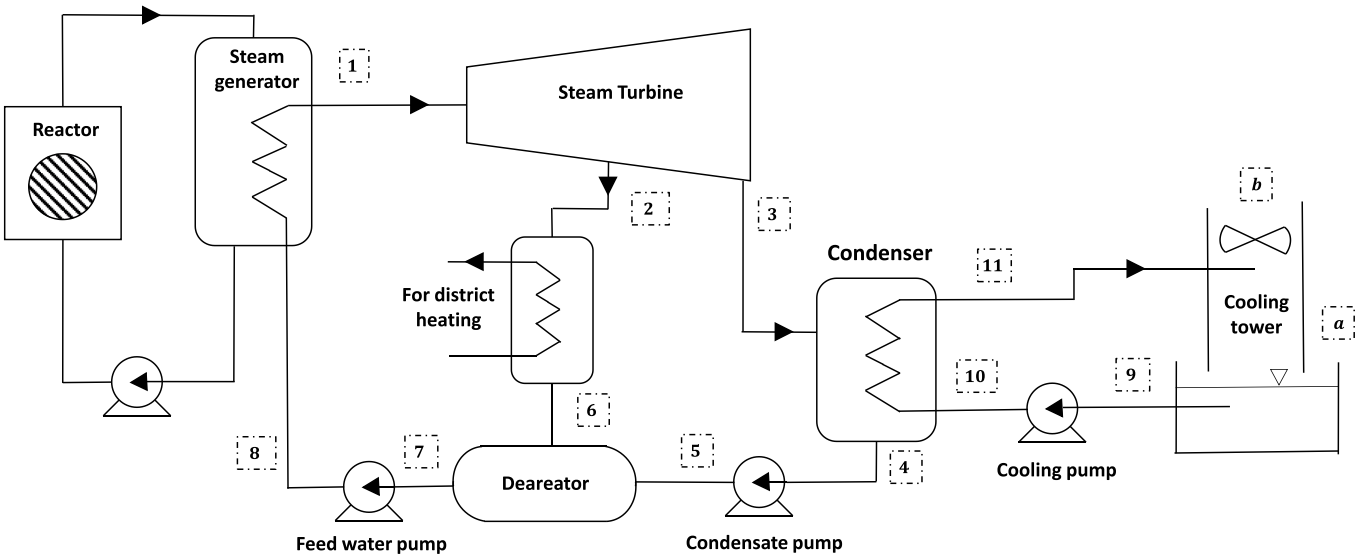

Fig. 4. Scheme of the HTR-10 with RRC

preheats the feed water before it enters the steam generator. The steam exiting the turbine (3) is condensed (4) in a closed heat exchanger where the steam is cooled by means of a water circuit including a cooling tower. In that circuit the cold water coming from the tower (9) is pumped and enters the at the condenser at (10). The temperature of the water at that point is called cooling temperature. Hot water leaving the condenser (11) is introduced in the cooling tower to be cooled by means of the air that flows at countercurrent. Air enters the tower at ambient conditions (a), and exits it (b) warmer and with higher humidity than at the inlet.

Fig. 5 shows the scheme of the HTR-10 but instead of using a RRC, the HCT is used for taking advantage of the benefits of the novel technology, and particularly, the savings of water consumption for cooling. The main differences between the cycles are that in HCT, condensation is performed in an absorber (an open heat exchanger) and it is produced mainly by absorption instead of conduction and convection mechanisms. Hygroscopic compounds dissolved in water are needed to that end. In the absorber, the pure steam coming from the turbine (1) and the solution with a low concentration of hygroscopic salts (15) get in contact, giving rise to condensation by absorption. The condensate exits the absorber as saturated liquid (4). In actual installations [76], the concentration is lower than 0.01 % and it is provided by the stream of purges extracted from the steam generator. It contains impurities that are hygroscopic and despite the fact that the concentration is very low, the mass flow rate of that stream is calculated to ensure the condensation by absorption in the absorber. These impurities are the real salts found in mains water and are used in actual HCT on an industrial scale. For this low concentration of salts, the values of the properties for

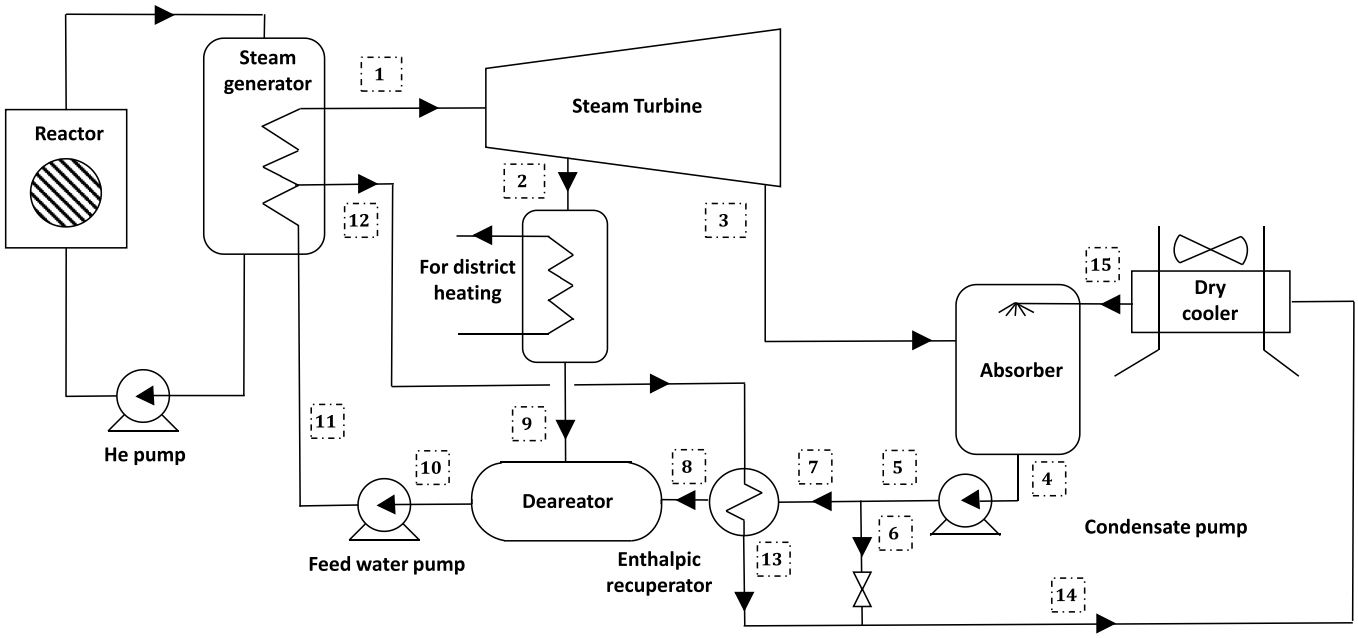

Fig. 5. Scheme of the HTR-10 with HCT

dissolution can be approximated by those of pure water. Besides, the energy of the purges stream (12) is recovered in the enthalpic recuperator (closed heat exchanger) for preheating the feed water before the deaerator (7, 8). Another important difference between the RRC and the HCT is that the later do not need cooling towers and the working fluid is cooled by dry coolers even at ambient temperatures higher than 40 °C. It is due to the condensation by absorption and the proper configuration of the cycle (Fig. 5). According to the design of the HCT, the temperature at (14) is approximately equals to the temperature at the absorber outlet (4). Notice that the cooling circuit is a closed loop. The mass flow rate corresponding to states (14) and (15) is also called cooling reflux. The temperature at the outlet of the dry coolers is called cooling temperature (15).

For developing the analytical models, mass and energy balances at steady-flow conditions are given by Eqs. (1) and (2) have been applied to each element of the cycles considered as a control volume (CV).

$$\sum_{in}\dot{m}_i = \sum_{out}\dot{m}_i \tag{1}$$

$$\dot{Q} - \dot{W} = \sum_{out}\dot{m}_i\left[h_i + \frac{c_i^2}{2} + gz_i\right] - \sum_{in}\dot{m}_i\left[h_i + \frac{c_i^2}{2} + gz_i\right] \tag{2}$$

where: $\dot{m}_i$ is the mass flow rate of the streams; h_i, c_i and z_i are the specific enthalpy, the velocity, and the elevation of the fluid at the inlets/outlets respectively; g is the gravity; $\dot{Q}$ and $\dot{W}$ are the heat transfer rate and mechanical power exchanged between the CV and the surroundings respectively.

Expressing the second member of Eq. (2) as $\Delta\dot{E}$, this can be rewritten as Eq. (3):

$$\dot{Q} - \dot{W} = \Delta\dot{E} \tag{3}$$

For the calculation of the variables in the cooling tower, psychrometric properties of humid air [87] have been considered. Humid air can be considered as an ideal-gas mixture whose pressure (P) is the sum of the partial pressure of dry air (P_a) and that of water vapor (P_v). It is obtained from Eq. (4).

$$P = P_a + P_v \tag{4}$$

Absolute humidity (w) can be obtained by Eq. (5).

$$w = \frac{m_v}{m_a} = 0.622\frac{P_v}{P_a}\ \text{(kg water vapor / kg dry air)} \tag{5}$$

Relative humidity ($\varnothing_a$) is the ratio amount of moisture the air holds (m_v) relative to the maximum amount of moisture the air can hold at the same temperature (m_g). It can be calculated by Eq. (6).

$$\varnothing_a = \frac{m_v}{m_g} = \frac{P_v}{P_g} \tag{6}$$

P_g is the saturation pressure at the air temperature.

The total enthalpy of humid air is the addition of the enthalpies of dry air and the water vapor (Eq. (7)).

$$H = m_a h_a + m_v h_v \tag{7}$$

For the mass and energy balances in the tower, it is considered that the air leaves the tower as saturated air.

Fig. 6 shows the scheme of the cooling tower of the RRC. It is a forced

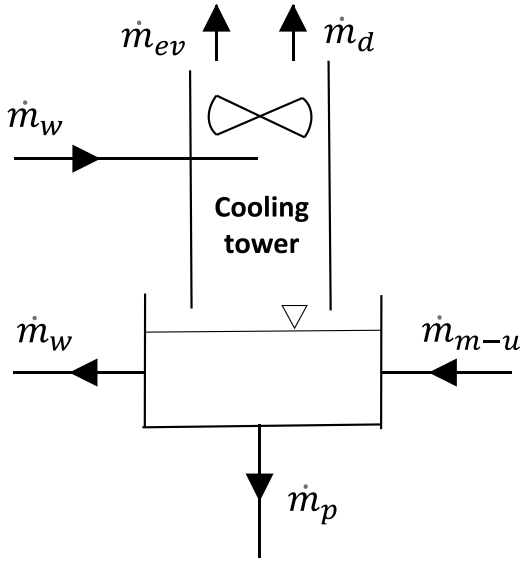

Fig. 6. Scheme of the RRC cooling tower.

draft cooling tower in which the water flows down and the air rises. The different mass flow rates of water are also indicated in that Figure. $\dot{m}_w$ is the mass flow rate of cooling water passing throw the condenser.

There is also a mass flow rate of purges ($\dot{m}_p$) needed to avoid scale. It is a percentage of the water inlet ($\dot{m}_w$). According to Ref. [88], that percentage is 0.7 %. $\dot{m}_{ev}$ is the mass flow rate of water evaporated and is obtained by Eq. (8).

$$\dot{m}_{ev} = \dot{m}_{v,out} - \dot{m}_{v,in} = \dot{m}_a(w_{out} - w_{in}) \tag{8}$$

Being $\dot{m}_a$ the mass flow rate of air passing through the tower.

The water droplet dragging mass flow rate ($\dot{m}_d$) depends on the type of droplet separator installed in the cooling tower. In this case it is a medium efficiency separator, and according to Ref. [88] this flow rate is 0.01 % of the main water mass flow rate ($\dot{m}_w$).

The mass flow rate of make-up water ($\dot{m}_{m-u}$) is obtained by Eq. (9).

$$\dot{m}_{m-u} = \dot{m}_p + \dot{m}_{ev} + \dot{m}_d \tag{9}$$

with the mass flow rate of make-up water, annual water consumption is calculated for 8000 h of plant operation.

2.3. Base cases definition

For the thermodynamic comparison of the cycles, actual data from the existing HTR-10, have been used. Those data have been detailed in Table 3.

2.4. Validation of the analytical data

The EES software has been widely used in the literature for the calculation of Rankine Cycles because it contains an accurate database of the most used working fluids in this cycle and the results obtained are very accurate [89–91]. In this work, calculations for RRC have been carried out with EES, obtaining results with differences lower than 2.5 % with respect to the actual data for the base case provided in the literature [84,85].

To validate the calculations for the HCT, also developed with the EES software, the calculated data are compared with experimental data obtained from a pilot plant of the HCT. This pilot plant is a reduced scale model of the HCT. It contains a 100-kW gas-fired boiler with a maximum capacity of 110 kg/h of steam at 200 °C and 14 bar. The scale of the plant allows for over 30 kW of power production. Details of the pilot plant, including equipment and uncertainties, have been published in Refs. [77,78].

2.5. Comparative analysis of RRC and HCT

A base case of the HTR-10 with an RRC was defined according to the data presented in the literature. In addition, a base case with the HCT has been defined for comparison, keeping the same input data (Table 3). The ambient temperature is assumed to be 20 °C. In the case of the RC, the Condenser Approach is 5 °C and the condensate is subcooled by 3 °C at the condenser outlet. Maximum relative humidity of the inlet air of the cooling tower is 80 %. The range of condensing pressure allowed is from 0.07 to 0.21 bar. The value of the cooling tower Approach is 3 °C. For covering the different actual District Heating (DH) demands, the mass flow rate of the bleeding ranges between 3000 and 4500 kg/h. Consequently, the study also includes the analysis of the variation of the bleeding mass flow rate within that range. Parameter (∅) determines the fraction of the live steam mass flow rate ($\dot{m}_{lv}$) that is extracted ($\dot{m}_{bd}$) for the thermal power production for DH.

$$\varnothing = \frac{\dot{m}_{bd}}{\dot{m}_{lv}} \tag{10}$$

Base cases of both RRC and HCT are compared including energy balances of the equipment, T-s diagrams and Sankey diagrams. In addition, thermal power provided for DH, net mechanical power produced, and mechanical power consumption of pumps and fans are analyzed for both cycles within the range of bleeding mass flow rate mentioned. On top of that, the cooling water savings obtained when the RRC is replaced by the HCT is quantified as a result of avoiding the used of cooling towers.

Base cases of both RRC and HCT are compared, including equipment energy balances, T-s diagrams, and Sankey diagrams. In addition, the thermal power provided for DH, the net mechanical power produced, and the mechanical power consumption of pumps and fans are analyzed for both cycles within the aforementioned bleeding mass flow range. Moreover, the cooling water savings obtained by replacing the RRC with the HCT are quantified as a result of avoiding the use of cooling towers.

Once the comparison of the base cases is done, a sensitivity analysis of the thermal power provided for DH, net and power consumption mechanical powers, and cooling mass flow rate of the cycles is performed varying different key parameters. Also, the analysis of cooling water savings for each case is quantified. The parameters varied for the sensitivity analysis are the condensing pressure (from 0.07 to 0.21 bar), the bleeding mass flow rate (from 3000 to 4500 kg/h), the relative humidity (from 0 to 100 %) and the ambient temperature (from 5 to 45 °C).

Table 3
HTR-10 thermodynamic data [84,85].

Steam Generator	
Inlet water temperature (°C)	104
Inlet water pressure (bar)	51
Outlet steam temperature (°C)	435
Outlet steam pressure (bar)	34.3
Steam mass flow rate (kg/s)	3.49
Turbine	
Exhaust steam temperature (°C)	41
Exhaust steam pressure (bar)	0.078
To district Heating	
Temperature (°C)	250
Pressure (bar)	5
Mass flow rate (kg/h)	3750

3. Results and analysis

3.1. Experimental contrast

The HCT calculations were validated with the experimental data obtained in the pilot plant. To define the data sets under different operating conditions of the HCT, the analytical values obtained with EES and the data from the pilot plant were compared for 3 different pressures for the boiler ($P_b = 8$, 10 and 12 bar). Table 4 shows the mass flow rates of live steam and boiler purges stream used for each pressure. The maximum temperature of the steam (T_{max}) (at the boiler outlet) is also shown in Table 4 for each pressure. The discrepancies between analytical and experimental values for these variables were less than 1.9 % (Table 4).

Figs. 7 and 8 show both analytical and experimental values of the bleeding mass flow rate ($\dot{m}_{bd}$) and the cooling reflux ($\dot{m}_r$) vs. condensing pressures (P_c) ranging from 0.05 to 0.15 bar and for the steam generator pressures mentioned. Finally, Fig. 9 shows the values of the cooling (T_r) and condensing (T_c) temperatures for the above pressures. In all cases, the discrepancies between the analytical and experimental values are all less than 2.1 %, so there is good agreement between the analytical and experimental data.

3.2. Base cases comparison

Figs. 10 and 11 present the T-s diagrams of both regenerative Rankine and Hygroscopic cycles for the base cases according to Figs. 4 and 5. In these cycles, the states corresponding to the turbines and steam

Table 4
Data for the validation of the HCT analytical model.

	$\dot{m}_{lv}$ (kg/h)			T_{max} (°C)			$\dot{m}_p$ (kg/h)		
P_b (bar)	analytical	experimental	error (%)	analytical	experimental	error (%)	analytical	experimental	error (%)
12	110.00	109.10	0.82	188.00	187.60	0.21	2.00	1.98	1.01
10	100.00	100.80	0.79	179.90	178.89	0.56	1.82	1.79	1.68
8	90.00	89.30	0.78	170.40	169.40	0.59	1.64	1.61	1.86

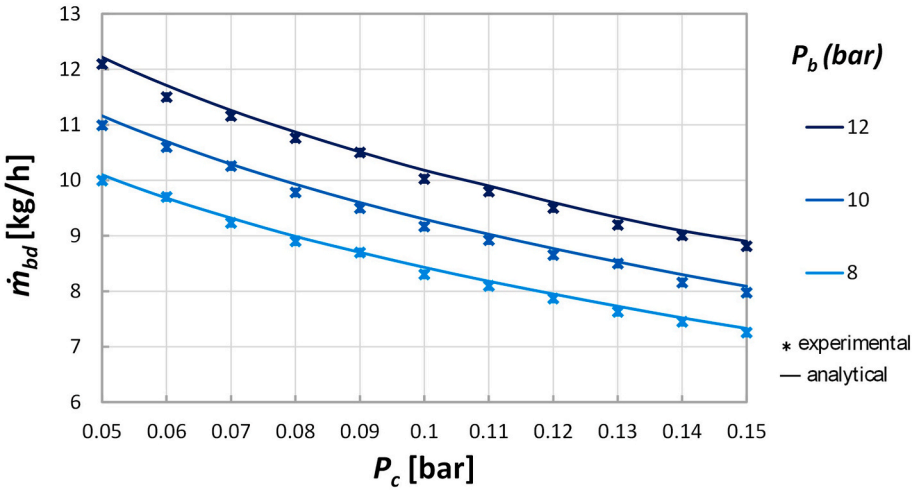

Fig. 7. Analytical and experimental values of the bleeding mass flow rate vs. condensing pressure for different boiler pressures of the HCT.

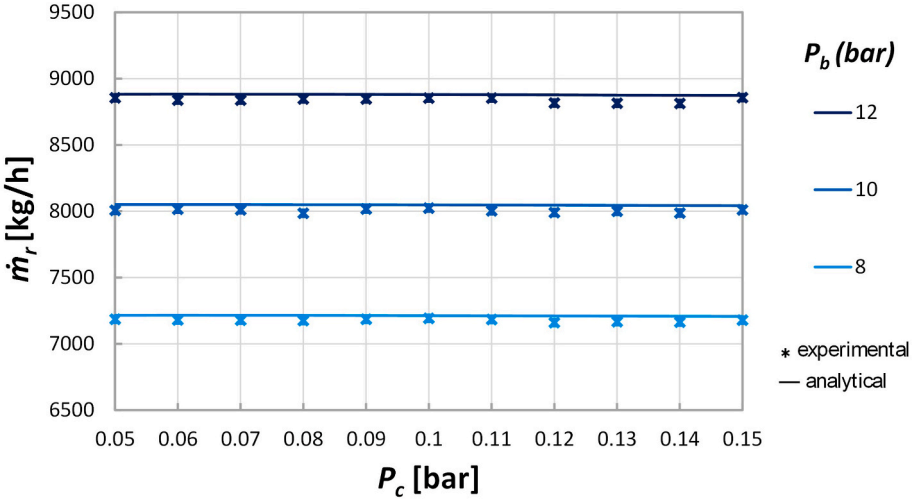

Fig. 8. Analytical and experimental values of the cooling reflux vs. condensing pressure for different boiler pressures of the HCT.

generators are identical, the main difference being that state 12 corresponds to the purge stream in the case of the HCT, while for the RRC there is no purge stream. Since the condensate of the RRC is subcooled at the outlet of the condenser, state 4 in the T-s diagram of the RRC is slightly lower than that of the HCT. Obviously, the states corresponding to the cooling systems are different in both cycles due to the different layouts. In Fig. 11, the region of the condensate including the cooling reflux (states 14 and 15) is enlarged because the states are very close to each other.

[92] presents a theoretical study of RC with reheating in a power plant, including the T-s diagrams. The T-s diagrams shown in Figs. 1 and 2 are coherent with the results presented in that study. RC is a well-known power cycle, and the diagrams are also widely studied along the years. Other references for validating the results obtained in the present paper are [45, 93].

Tables 5 and 6 show the energy balances of the different equipment for both cycles. The thermal power supplied to both of them is 10 MW, according to the specifications of the HTR-10. The gross mechanical power produced by the turbines is the same for both cycles, but the power consumption of the fans and pumps is higher for the HCT. This is due to the higher power consumption of the fans in the RRC cooling tower. It is more than double that of the dry cooler fans. Note that the consumption of the condensate pump in the HCT is much higher than that of the RRC because the mass flow passing through the former is the addition of feed water and cooling reflux (a total of 115.3 kg/s), while for the RRC the mass flow rate is only that of feed water (2.45 kg/s). As a result of the lower total mechanical power consumption in the HCT, the net power production of 2322.11 kW, 0.58 % greater than that of the

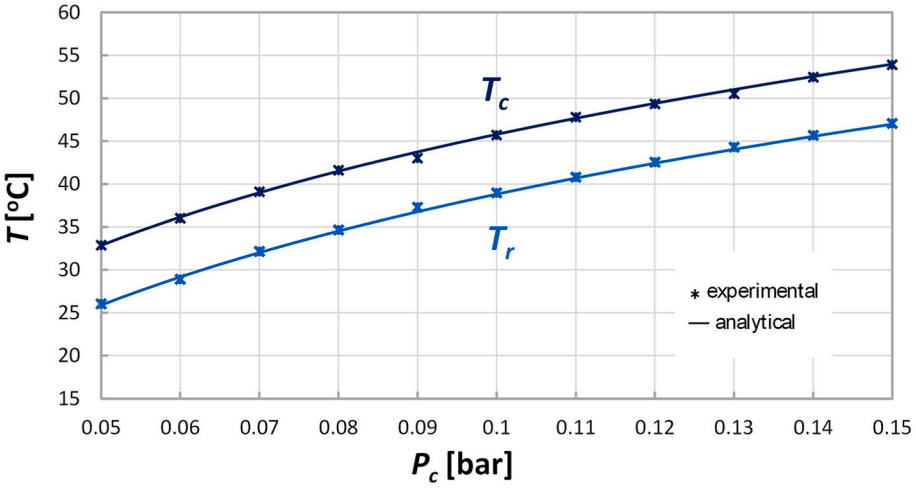

Fig. 9. Analytical and experimental values of the cooling and condensing temperatures vs. condensing pressure of the HCT.

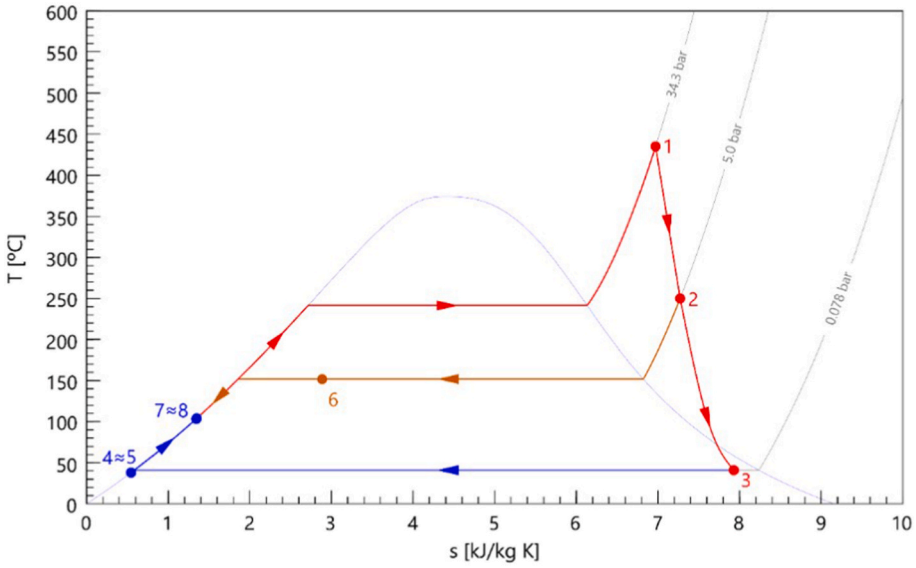

Fig. 10. T-s diagram of the RRC base case.

RRC. In addition, the thermal power produced by the HCT is of 1994 kW, 1.59 % greater than that of the RRC, for the same operating conditions.

Figs. 12 and 13 show the Sankey diagrams of RRC and HCT, respectively. The diagrams detail the energy flows per unit time between the equipment for each cycle. In the HCT, the energy content per unit time of the purge stream is quite low (18 kW), but it is necessary to provide the hygroscopic compounds in the cooling reflux and thus the necessary condensation of water by absorption in the absorber. Most of the power of the purge stream is recovered in the recuperator heat exchanger to preheat the feed water, leaving only 2.1 kW for the connection to the cooling system. It should be noted that the desorption of the hygroscopic compounds takes place in the drum of the steam generator, thus providing a purge stream with a concentration of hygroscopic compounds lower than 0.01 %, according to the industrial plants already in operation.

Energy balances presented in Tables 5 and 6 and Sankey diagrams are coherent with those published in Refs. [93–95].

The main difference between RRC and HCT is the cooling system. According to the Sankey diagrams, the thermal power content of the flows is greater in the HCT, due to the correct layout of this cycle and also because condensation is carried out by absorption with subsequent increase in temperature by ebullioscopic effect. Despite the fact that this ebulloscopic increase is very small for the low concentrations of hygroscopic salts considered in this study, these concentrations are sufficient for condensation by absorption to take place in the absorber. This gives rise to a condensate at the outlet of the absorber at a temperature (slightly higher than that of water saturation at the absorber pressure), but which in any case is much higher than that obtained in a RRC at the outlet of the condenser. It provides higher temperature values in the HCT cooling system than in the RRC, and therefore at higher temperature values in the HCT cooling system than in the RRC. As a result, the heat is released under better conditions than in the RRC, allowing the use of dry coolers and eliminating the need for cooling towers and make-up water consumption, for a wide range of ambient temperatures.

A sensitivity analysis of the base cases is performed considering the regulation of the bleeding mass flow rate to provide the required thermal power when the DH demand varies according to the technical specifications of the HTR-10. Fig. 14 shows the fraction of the bleeding mass flow rate (⌀) within the range indicated in the specifications of the HTR-10. It ranges from 23.88 to 35.81 % of the live steam mass flow rate. For the base cases already studied, the value was 29.85 %. Fig. 15 shows the comparison of net mechanical power and thermal power

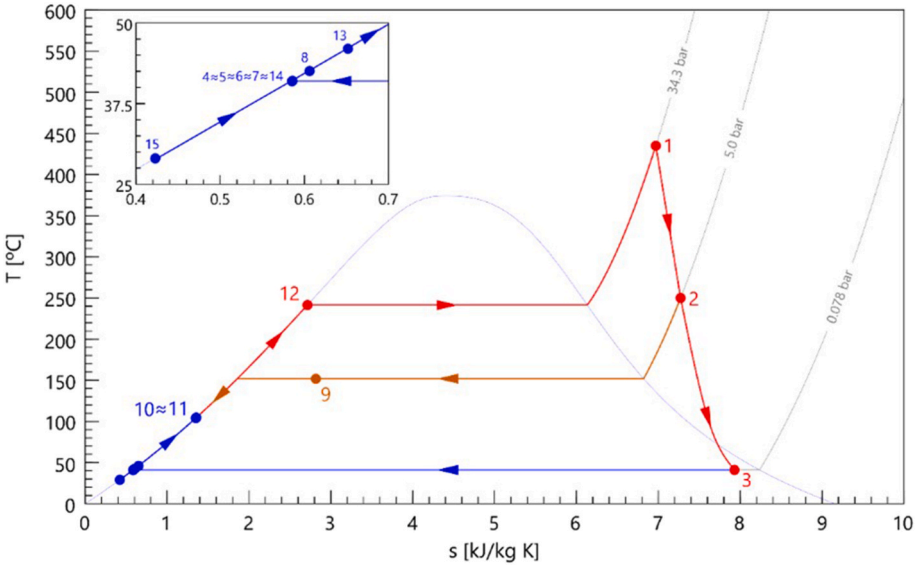

Fig. 11. T-s diagram of the HCT base case.

Table 5
Energy balances in the equipment of the RRC base case.

RRC	$\Delta\dot{E}$	$\dot{Q}$	$\dot{W}$
Steam Generator	10000.00	10000.00	0.00
Turbine	−2382.00	0.00	2382.00
Condenser (steam)	−5680.20	−5680.20	0.00
Condenser (cooling water)	5680.20	5680.20	0.00
Condensate pump	0.90	0.00	−0.90
Deaerator	0.00	0.00	0.00
Heat exchanger for DH	−1962.70	−1962.70	0.00
Feed water pump	24.00	0.00	−24.00
Cooling pump	12.00	0.00	−12.00
Cooling Tower	36.39	0.00	−36.39
Total	5728.59	8037.30	2308.71

Table 6
Energy balances in the equipment of the HCT base case.

HCT	$\Delta\dot{E}$	$\dot{Q}$	$\dot{W}$
Steam Generator	10000.00	10000.00	0.00
Turbine	−2382.00	0.00	2382.00
Absorber	0.00	0.00	0.00
Condensate pump	18.00	0.00	−18.00
Recuperator	0.00	0.00	0.00
Deaerator	0.00	0.00	0.00
Heat exchanger for DH	−1994.00	−1994.00	0.00
Feed water pump	24.10	0.00	−24.10
Dry cooler (working fluid)	−5666.10	−5666.10	0.00
Dry cooler (air)	5682.45	5666.10	−16.35
Total	5682.45	8006.00	2322.11

production for the base cases, but with different bleeding mass flow rates. The net mechanical power provided by the HCT is between 0.5 and 0.7 % higher than that of the RRC under the same conditions. In addition, the mechanical power decreases as the bleeding mass flow rate increases because less mass flow passes through the low-pressure turbine. Similarly, the thermal power for DH is between 1 and 2.5 % greater in the HCT, with the opposite trend as for the net mechanical power.

The enthalpy of the extraction (inlet of the heat exchanger) is the same in all cases, and the enthalpy at the outlet of the heat exchanger is practically identical for RRC and HCT as a result of the energy conservation in the deaerator. Consequently, the effect of increasing the bleeding fraction on thermal power for DH is due to the increment of mass flow rate derived to the heat exchanger for DH purposes. Note that the differences between HCT and RRC become smaller for both types of power as the bleeding mass flow rate increases, so in this sense the influence of bleeding is greater in HCT.

Fig. 16 shows the comparison of the mechanical power consumption of the consumers (fans and pumps) and the cooling mass flow rate (cooling reflux in HCT) for the base cases, but with different bleeding mass flow rates. Power consumption and mass flow rates decrease as the bleeding rate increases because the pumping mass flow rates become lower. Consumption is 18–22 % higher for the RRC, and the difference decreases as the bleeding increases. Cooling mass flow and cooling reflux follow similar trends, but with fairly small differences (between 0.31 and 0.33 %). To perform a more in-depth analysis of the power consumption, for the RRC, the consumers with the higher percentage of consumption are the fans of the cooling tower (about 50 %), the feed water pump (33 %); while the consumption percentage is around 16 % and 1 % for the cooling and condensate pumps, respectively. In the case of the HCT, the consumption percentages are 41 %, 31 % and 28 % for the feed water pump, the condensate pump, and the fans of the dry coolers, respectively. Consequently, the distribution of the percentages among the different consumers is more homogeneous for the HCT than for the RRC, so that the consumers have a similar influence on the power consumed. On the contrary, the fans of the cooling tower account for about half of the consumption of the RRC. The consumption of condensate pump for the RRC is very low compared with the one of the HCT, because the mass flow rate passing through the pump of the latter (at the outlet of the absorber) is much greater than that of the former (at the outlet of the condenser). Note that the mass flow rate of the condensate at the absorber outlet includes the cooling reflux due to the layout of the HCT. It is also important to remark that the consumption of the fans of the HCT is much lower than that of the RRC, which is one of the most important advantages of the HCT. As regards consumption of the feed water pumps, they are similar in both, RRC and HCT (mass flow rates and enthalpy changes are similar); but in percentage, the consumption of those pumps is greater for the HCT because the total consumption is lower.

Regarding water consumption in the RRC, Fig. 17 shows the m^3 of make-up water per year that must be provided to the cycle in order to compensate the losses of water in the cooling tower (purges, evaporation and water droplet dragging). According to the data obtained, the mass flow rate of water evaporated is about 1.6 % of the cooling mass flow rate and accounts for the maximum percentage of the make-up water.

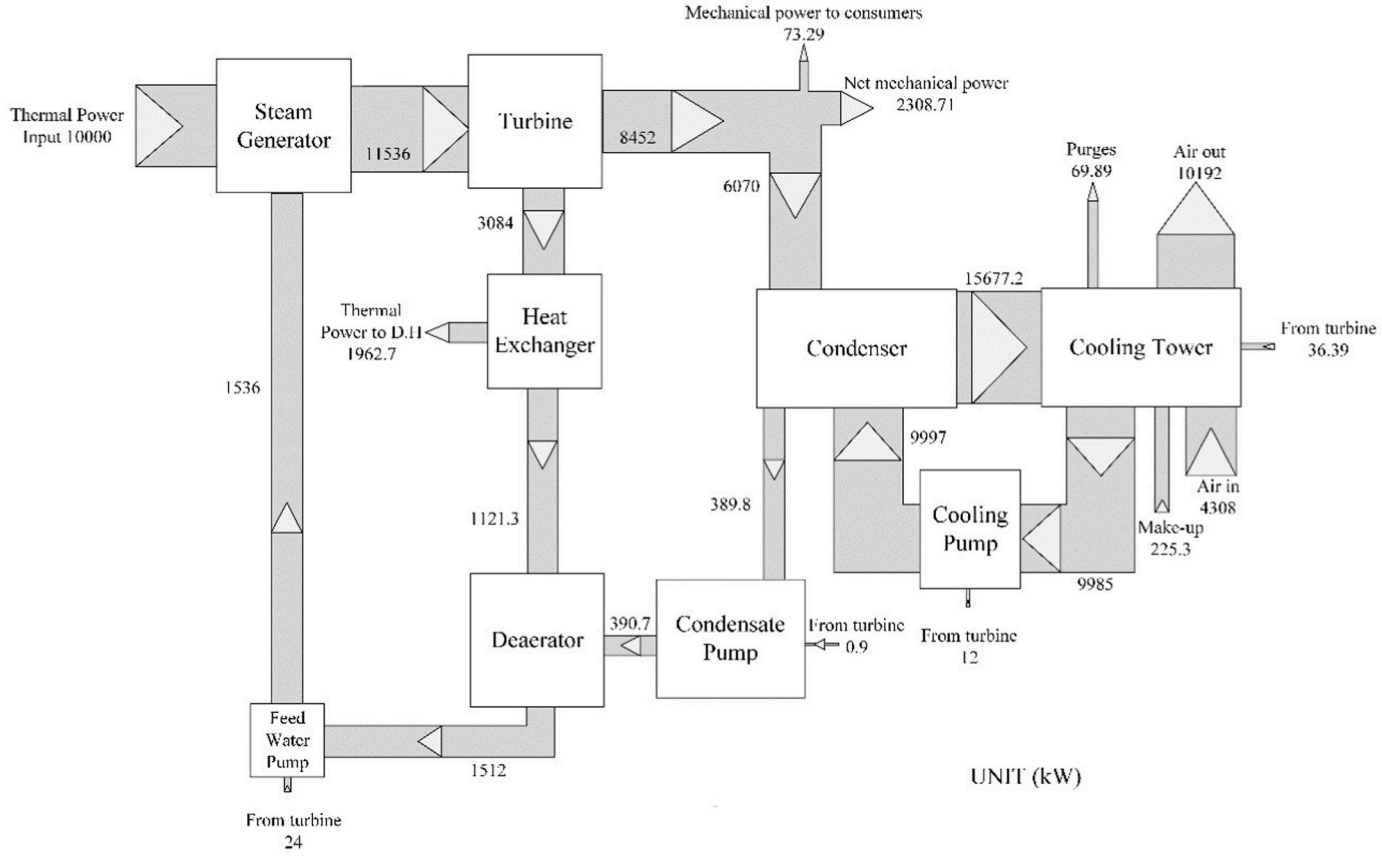

Fig. 12. Sankey diagram of the RRC base case.

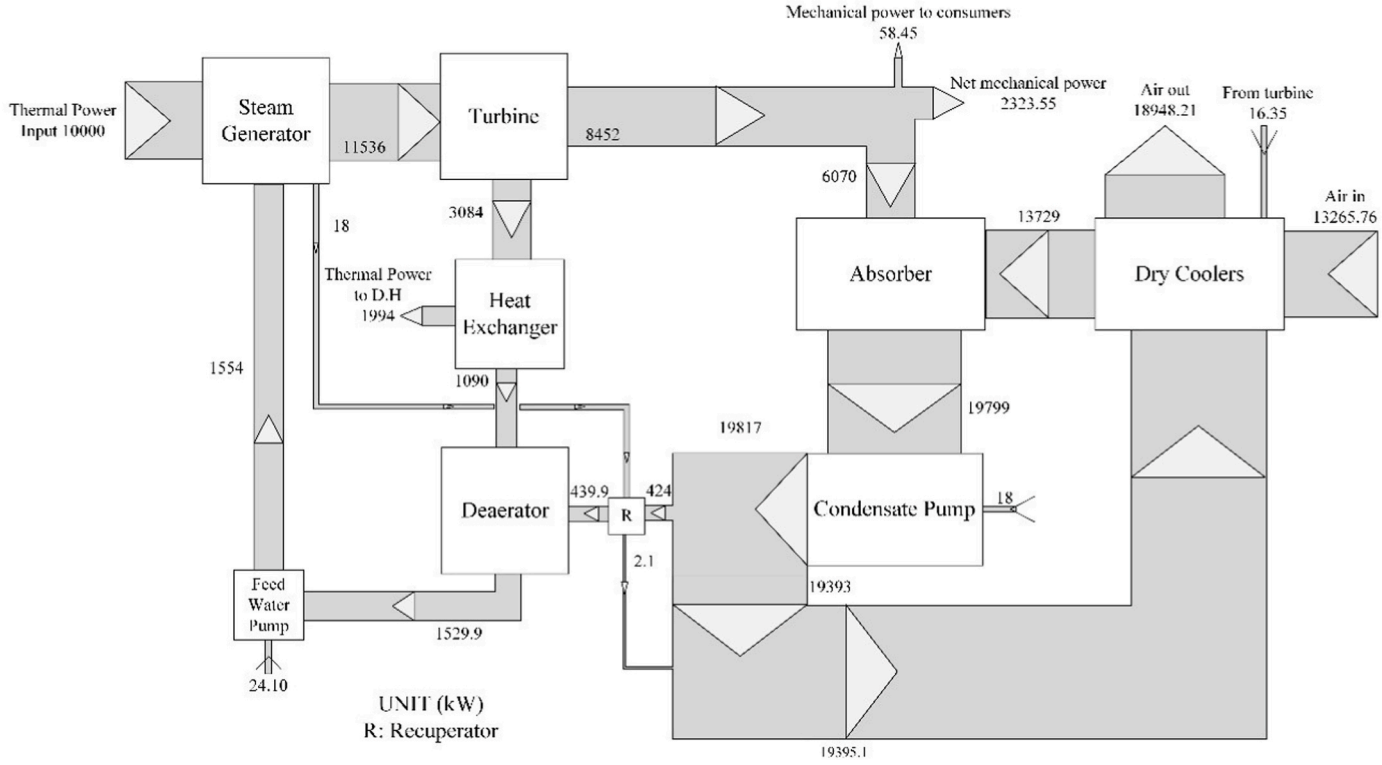

Fig. 13. Sankey diagram of the HCT base case.

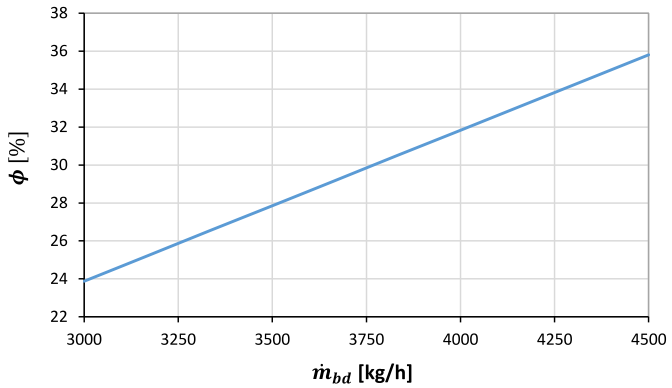

Fig. 14. Bleeding fraction mass flow rate vs. bleeding mass flow rate for both RRC and HCT.

The other mass flow rates included in the make-up have smaller percentages of the cooling flow rate, as explained in the methodology. Consequently, when the bleeding mass flow rate is increased, cooling flow rate is decreased (Fig. 16), and both the mass flow rate of make-up water and the water consumption are also lowered. For the calculation, 8000 h of functioning per year have been considered. It varies between 70683.4 and 83842.6 m^3/year. Consequently, the incorporation of the HCT would save a considerable amount of water, in addition to improving cycle performance.

3.3. Other sensitivity analyses

Fig. 18 shows the effect of condensing pressure on the DH thermal power for the (a) HCT and (b) RRC. According to these results, the thermal power increases as the condensing pressure increases. It is greater for the HCT for each bleeding rate and condensing pressure considered. The increase varies from 1 to a maximum of 2.5 % with respect to RRC for the cases studied. In addition, the higher the bleeding rate, the lower the increase in thermal power with respect to RRC. Also, the increase in thermal power for a fixed bleeding rate is lower between the lines of constant pressure as condensing pressure is increased. In both cycles the trends are similar, but the influence of the condensing pressure is slightly stronger in the HCT. The maximum thermal production for DH is 2762 kW for HCT (at higher condensing pressure and higher bleeding mass flow rate). Note that, for each bleeding mass flow rate, when condensing pressure decreases, the enthalpy of the condensate decreases as well, so the enthalpy at the outlet of the heat exchanger is increased for maintaining the optimum conditions in the deaerator (minimum solubility of gasses in the working fluid). Since the enthalpy at the inlet of the heat exchanger is fixed by the specifications of the cycle, the enthalpy change in the exchanger is decreased, and therefore, the thermal power available for DH is also lowered. On the other hand, when condensing pressure is fixed, both the enthalpy change in the heat exchanger and the thermal power for DH increase when increasing the bleeding mass flow rate.

Fig. 19 shows the effect of varying condensing pressure and bleeding mass flow rate on net mechanical power production for (a) HCT and (b) RRC. The trends are opposite to those for thermal power. The main

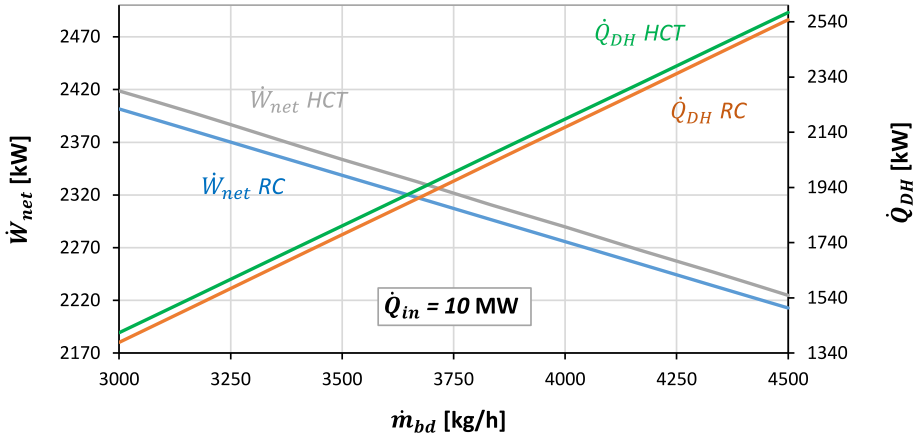

Fig. 15. Net mechanical power and thermal power production for DH vs. bleeding mass flow rate of RRC and HCT.

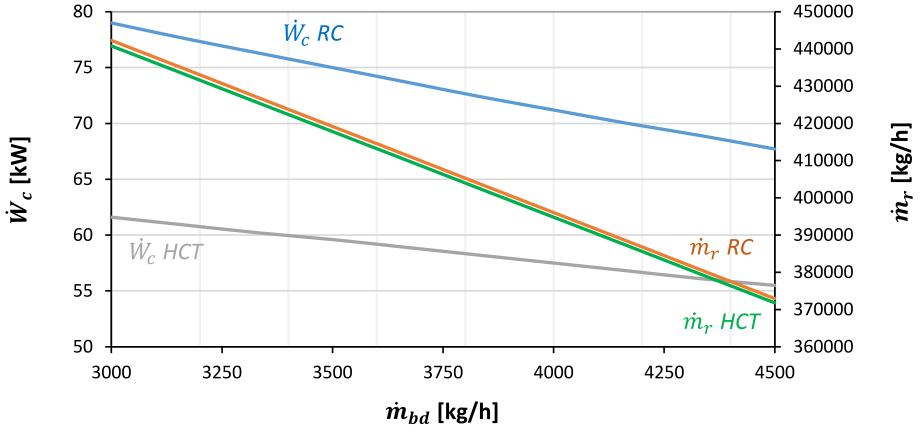

Fig. 16. Mechanical power consumption and cooling mass flow rate vs. bleeding mass flow rate of RRC and HCT.

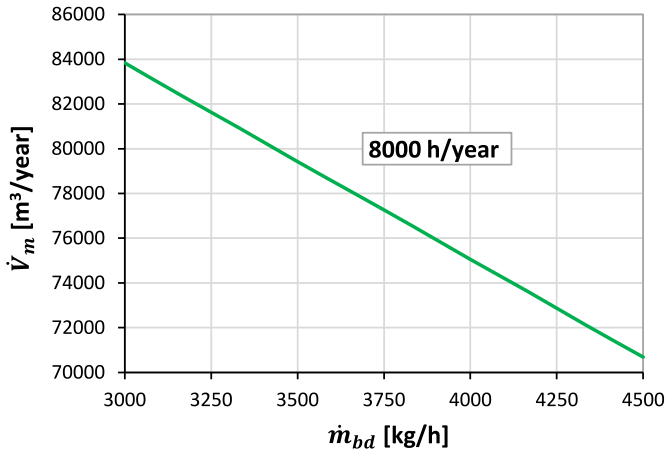

Fig. 17. Annual cooling water consumption vs. bleeding mass flow rate of the RRC.

reason is that the lower the condensing pressure, the higher the enthalpy difference between the turbine inlet and outlet for the same steam mass flow rates, and therefore the power production increases. The increase varies from 0.1 to a maximum of 1 % with respect to RRC for the cases studied. Maximum net mechanical power is of 2417 kW with the HCT (at lower condensing pressure and lower bleeding mass flow rate).

The results obtained for mechanical power consumption are shown in Fig. 20 (a) and (b) for HCT and RRC, respectively. According to these results, the trends are similar to those of the net power, but the increase in power consumption is greater as the condensing pressure decreases. This is due to the fact that the lower the condensing pressure, the higher the pressure change in the condensate pump and therefore, the power consumption increases. On top of that, for lower pressures, the temperatures of the working fluid are also lower, so the fans consumption increases. This effect is more pronounced in the RRC. The consumption is also higher for RRC than HCT for the operating conditions studied. The decrease in consumption of HCT when increasing the bleeding mass flow rate varies from 4.11 to 27.9 %, taking the higher values for lower condensing pressures.

[96,97] present parametric analyses of RRC, among other studies. Pressure ratio is used for the study. It is defined as ratio of turbine inlet pressure to turbine outlet pressure (condensing pressure). Therefore, an increase in the pressure ratio is equivalent to a lower condensing pressure in the present study (the pressure at the turbine inlet is fixed). According to their results, the efficiency of the cycle increases when the pressure ratio increases, so, when the condensing pressure is lowered. Since in the preset study the thermal power input is fixed, an increment in the efficiency means an increment in the net power. Note that in the present paper, the useful power output is the addition of the net mechanical power production and the thermal power for DH, but the effect of the net mechanical power is dominant according to the results obtained. Consequently, the results shown in Figs. 18–20 are corroborated by the references cited.

Fig. 21 (a) shows the cooling reflux of the HCT versus the bleeding mass flow rate for the different condensing pressures. Fig. 21 (b) also shows the RRC cooling mass flow rate values for the same conditions. In both figures, the region corresponding to the lower bleeding is zoomed in to better visualize the effect of condensing pressure. The effect of varying the pressure in the cooling flow rate and cooling reflux is similar for both cycles. According to the previous results, there are two opposite effects when the condensing pressure is increased, on the one hand, the thermal power for DH is increased; on the other hand, net power production decreases, but the magnitude of the latter is greater than that of the former. Since the thermal power input of the cycle is constant and according to the energy conservation principle, the heat to be released in the cooling system is increased, and the mass flow rate of the cooling systems is to be increased as well (enthalpy changes remain almost constant). Results show that the cooling reflux is between 0.29 and 0.32 % higher than the cooling flow rate of the RRC for the same bleeding and condensing pressure. The difference increases with increasing condensing pressure. In both cycles, the effect of condensing pressure is more pronounced at lower values of this variable. Note that the trends are similar to those of the thermal power for DH. The advantage in the case of HCT is that the cooling reflux is part of a closed circuit and there is no continuous make-up water.

Fig. 22 quantifies the water consumption per year for 8000 h of annual plant operation. This consumption increases as the condensing pressure increases, its effect being attenuated at higher pressures. The increase can be explained because the tendencies of the make-up mass flow rate are the same as those of the cooling reflux, according to the relation existing with the flow rate of evaporation, purges and water droplet dragging described in the methodology and in the previous results. The water consumption ranges from 70680 to 84656 m^3/year for the operating conditions studied. Consequently, this is the interval of

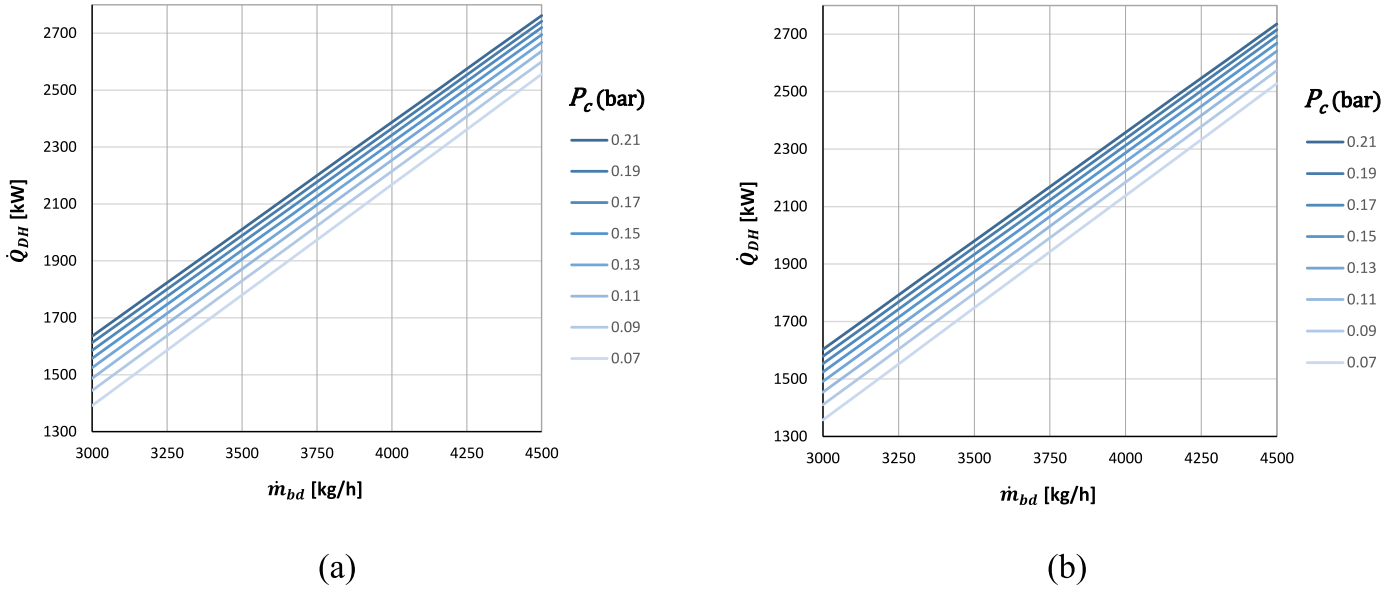

Fig. 18. Thermal power production for DH vs. bleeding mass flow rate at different condensing pressures for (a) HCT and (b) RRC.

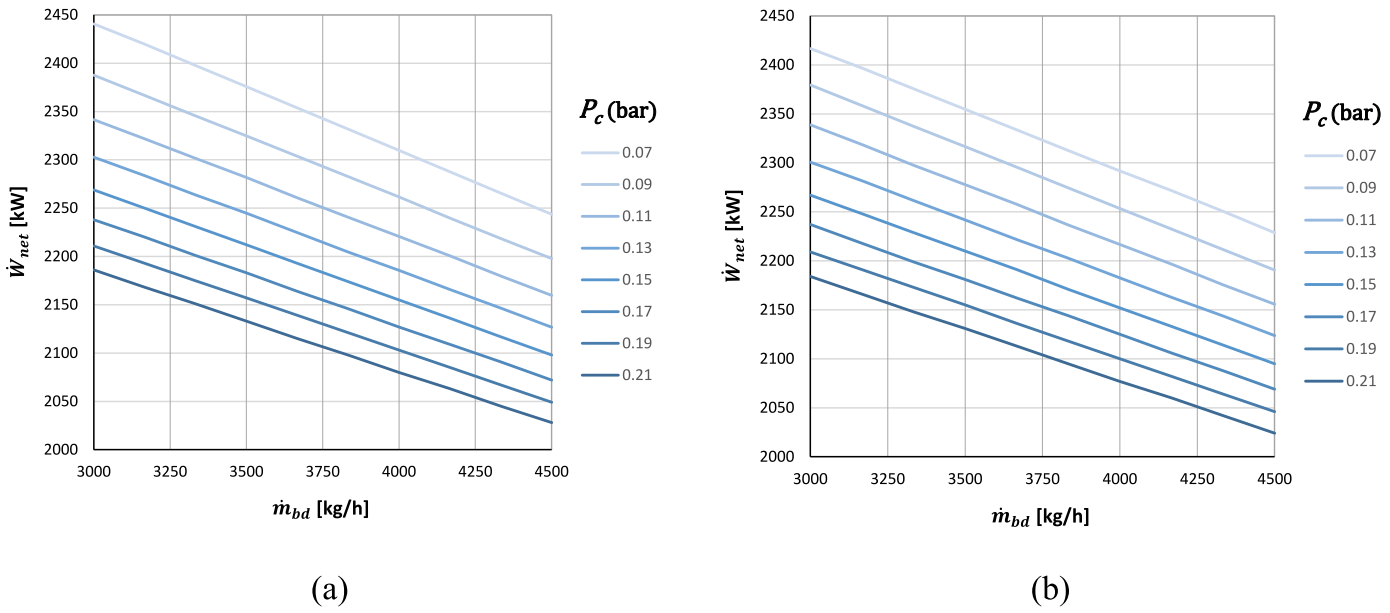

Fig. 19. Net mechanical power production vs. bleeding mass flow rate at different condensing pressures for (a) HCT and (b) RRC.

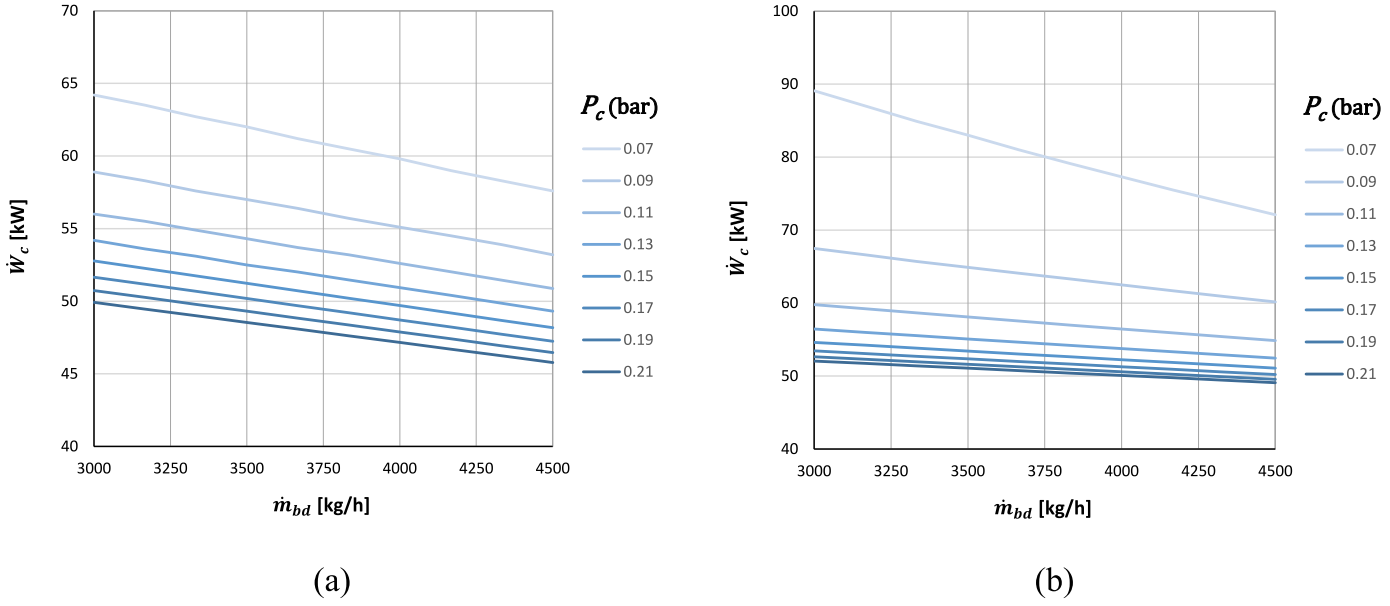

Fig. 20. Mechanical power consumption vs. bleeding mass flow rate at different condensing pressures for (a) HCT and (b) RRC.

potential water savings of the plant when using the HCT instead of the RRC.

Fig. 23 shows the cooling temperatures obtained for the different condensing pressures for both HCT and RRC. The cooling temperature of HCT is higher than that of RRC for each condensing pressure, due to the different layout of the cycles and the effect of condensation by absorption. The cooling temperature was calculated considering the condensing temperature for each pressure, the Approach of the condenser, and the temperature change in the cooling tower, for the RRC. In the case of the HCT, the condensing temperature is also the temperature inlet of the dry coolers and, therefore, the cooling temperature is equal to that temperature minus the temperature change in the dry coolers.

The Approach of the cooling tower is the difference between the wet temperature of the inlet air and the minimum temperature of the water to be cooled, which is also the cooling temperature at the inlet of the absorber. Consequently, depending on the dry temperature of the air and its humidity, there is a different minimum for the cooling temperature. Considering the data of the base case, the condensing pressure is 0.078 bar, the cooling temperature is 21 °C (Fig. 23) and the ambient temperature is 20 °C. Under these conditions, Fig. 24 shows the effect of the relative humidity of the ambient air on the following variables of the RRC: (a) net mechanical power produced; (b) mechanical power consumed by fans and pumps; (c) make-up water consumption. This graph also shows, the minimum cooling temperature is also plotted. It allows to determine the maximum relative humidity for the correct performance of the cooling tower. In this case, it is 82 % and therefore, the specifications of the HTR-10 are met (it must operate up to 80 %). With this value, the minimum net mechanical power (2295 kW), the maximum power consumption of the consumers (86 kW) and the minimum make-up water consumption (75200 m^3/year) are determined. For the maximum relative humidity allowed, the net power decreases

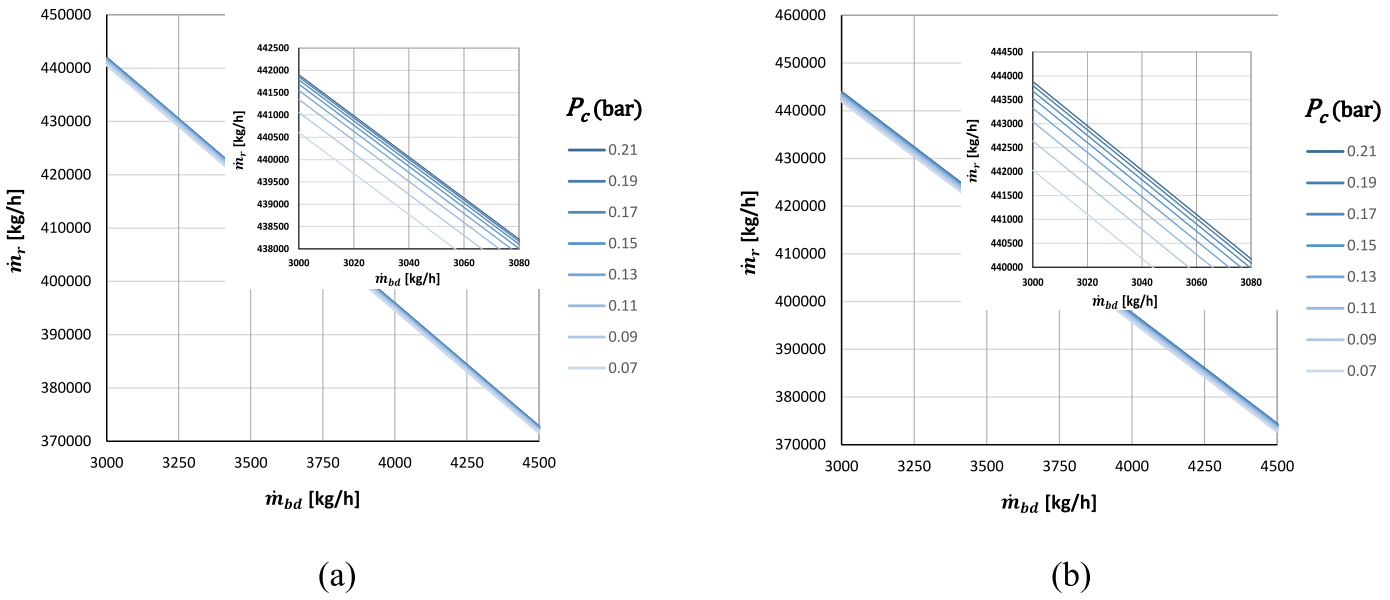

Fig. 21. Cooling mass flow rate vs. bleeding mass flow rate at different condensing pressures for (a) HCT and (b) RRC.

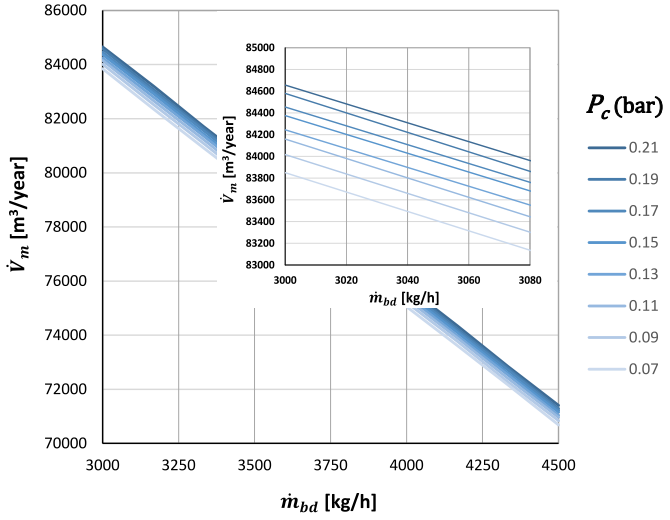

Fig. 22. Annual cooling water consumption vs. bleeding mass flow rate at different condensing pressures for the RRC.

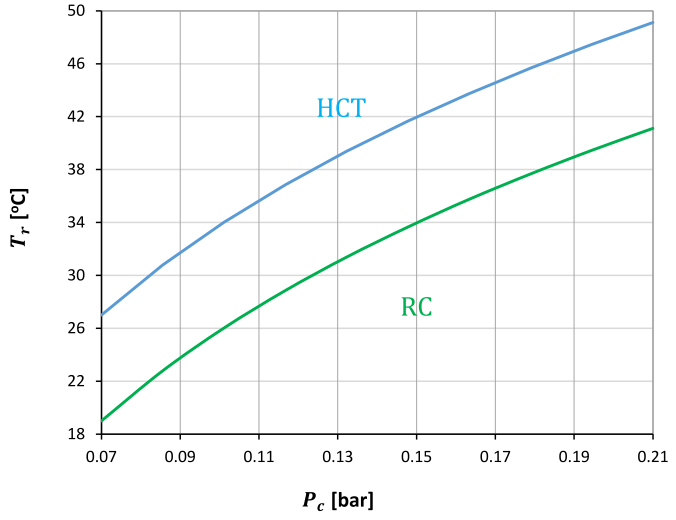

Fig. 23. Cooling temperatures of HCT and RRC vs. condensing pressure.

5.9 % and the water consumption decreases 2.75 %, with reference to 60 % humidity. The decrease of net power production when relative humidity increases is due to the increment of the cooling tower fans consumption. The water consumption decreases for higher humidities because the mass flow rate of water evaporated is lower.

The influence of the ambient temperature is shown in Fig. 25 for the same conditions as in Fig. 24, but with 60 % of the relative humidity. This figure shows that the maximum ambient temperature (temperature of the air at the inlet of the tower) is 23.5 °C. Under those conditions, 2300 kW, 90 kW and 80370 m^3/year are the minimum net mechanical power, the maximum power consumption of the consumers and the minimum make-up water consumption respectively. With the maximum ambient temperature allowed, the variations respect to 20 °C are 3.8 % decrease in net power and 3.9 % increase in water consumption. The net power production is lower as the ambient temperature increases because the fans consumption increases. The increment in the consumption of the fans when ambient temperature is increased is mainly due to the lower temperature difference between the air and the water to be cooled. The mass flow rate of make-up and the water consumption increase with the ambient temperature because the mass of water evaporated also increases (the needed mass flow rate of air passing through the cooling tower is greater).

The results can be corroborated by the study presented in Ref. [95]. They studied a combined cycle and concluded that the effect of the increase in ambient temperature in the RRC is almost negligible, compared to that of the gas turbine. The study was performed for a gas turbine of 45 MW and a steam turbine of 12 MW. In the present study, the power of the steam turbine is lower than 3 MW, so compared to the data of the combined cycle, the variation in power production of the RRC will be negligible as well.

For the HCT, the effect of the ambient temperature on the power production is shown in Fig. 26 for the base case (cooling temperature of 29 °C). In the HCT, the dry coolers operate at maximum when the temperature difference between the air and the cooling temperature is 6 °C, so when the cooling temperature is 29 °C, the maximum ambient temperature is 23 °C keeping the rest of operation conditions of the base case. According to Fig. 26, the minimum net power is 2315 kW (a decrease of 0.37 % with respect to the ambient temperature of the base case, 20 °C).

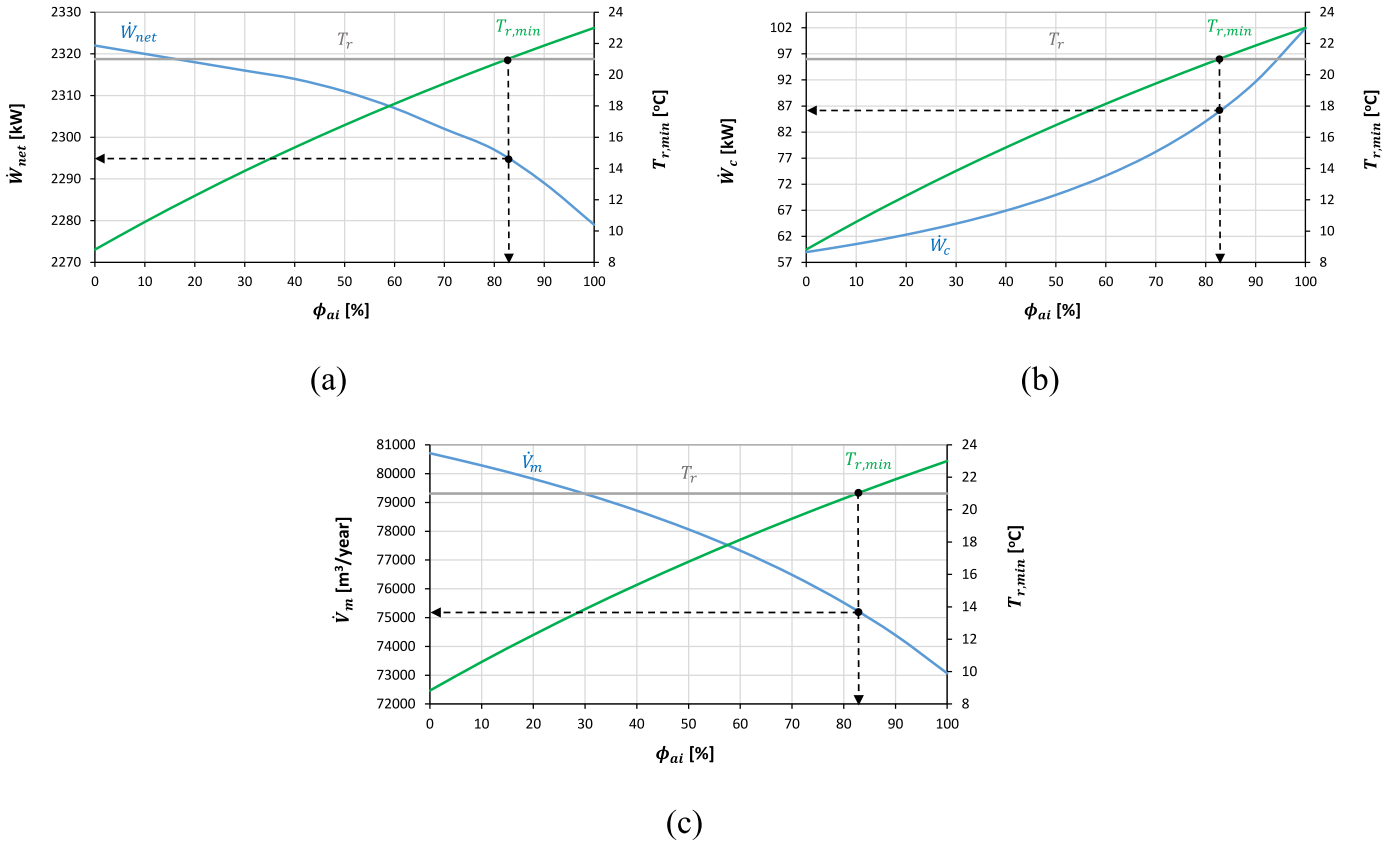

Fig. 24. Cooling temperature and (a) net mechanical power production, (b) mechanical power consumption, (c) thermal power production for DH vs. relative humidity of the ambient air for the RRC.

In order to determine the maximum ambient temperature for the RRC to operate within the HTR-10 specifications, operation of the plant at 80 % of relative humidity must be guaranteed. In addition, the maximum condensing pressure (0.21 bar) and the corresponding cooling temperature of the RRC (41.12 °C) must be considered. Fig. 27 shows the results obtained under the previous conditions and at 41.5 °C, that is the higher ambient temperature at which the minimum cooling temperature and maximum humidity conditions are met. According to Fig. 27, under the above conditions, the minimum net mechanical power, the maximum power consumption of the consumers and the minimum make-up water consumption are 2100 kW, 54.71 kW and 85758 m^3/year, respectively. Note that the maximum water consumption of the RRC can be more than 88000 m^3/year.

Note that for any given condensing pressure, condensation by absorption will occur in the absorber at a condensing temperature given by the Clausius-Clapeyron equation, with a very small ebullioscopic increment that is negligible for the very low salt concentration considered. The fluid exits the absorber as saturated liquid at this temperature. According to the design configuration of the HCT, the temperature at the inlet of the dry coolers will be equal to the condensation temperature, and therefore, since the temperature change in the dry cooler field has been set at 12 °C, the cooling temperature at the inlet of the absorber will be 12 °C lower than the condensation temperature. On the other hand, according to the design of the dry cooler field, the maximum admissible temperature difference between the outlet of that equipment and the ambient temperature for a proper operation is 6 °C. Therefore, the maximum ambient temperature that the cooling system can withstand is 18 °C lower than the condensation temperature. That is to say, the maximum ambient temperature will correspond to the maximum cooling temperature and the maximum tolerable condensation pressure. In this study, the maximum condensing pressure is 0.21 bar, and the maximum condensing temperature is 61.12 °C. According to the previous reasoning, the corresponding cooling temperature is 49.12 °C. Therefore, the dry cooler could operate up to an ambient temperature of 43.12 °C. Fig. 28 shows the dependence of the net power production with the ambient temperature for the HCT at the higher condensing pressure (0.21 bar). The net power produced with the HCT decreases as ambient temperature is increased due to the increment of power consumption of the fans. At the maximum ambient temperature, the net power produced with the HCT can be as low as 2094 kW, while that production can decrease down to 2100 kW, at the maximum ambient temperature with the RRC. The minimum net power production is very similar, but the maximum ambient temperature for the correct operation of the HCT is 1.62 °C higher than that of the RRC, thus the HCT increases the availability of the cycle and avoids a water consumption for cooling that can reach values greater than 88000 m^3/year with the RRC.

The results obtained are coherent with those presented in Refs. [98, 99]. According to those studies, the most relevant part of the water consumption in a cooling tower is due to evaporation, and it increases as the cooling mass flow rate is increased. In Ref. [100], a numerical simulation of a counterflow cooling tower was performed. Results show that the effect of an increment of the ambient temperature entails an increment of the mass flow rates, and therefore, of the water consumption.

4. Conclusions

The study of the implementation of HCT was carried out in an existing nuclear power plant with an HTR-10 reactor that operates with a regenerative Rankine cycle. The aim was to investigate the potential benefits of HCT in terms of energy production and water savings. The actual power plant was designed to produce both thermal energy for District Heating and electric power. Analytical models of the RRC and the HCT were developed using the EES software to meet the

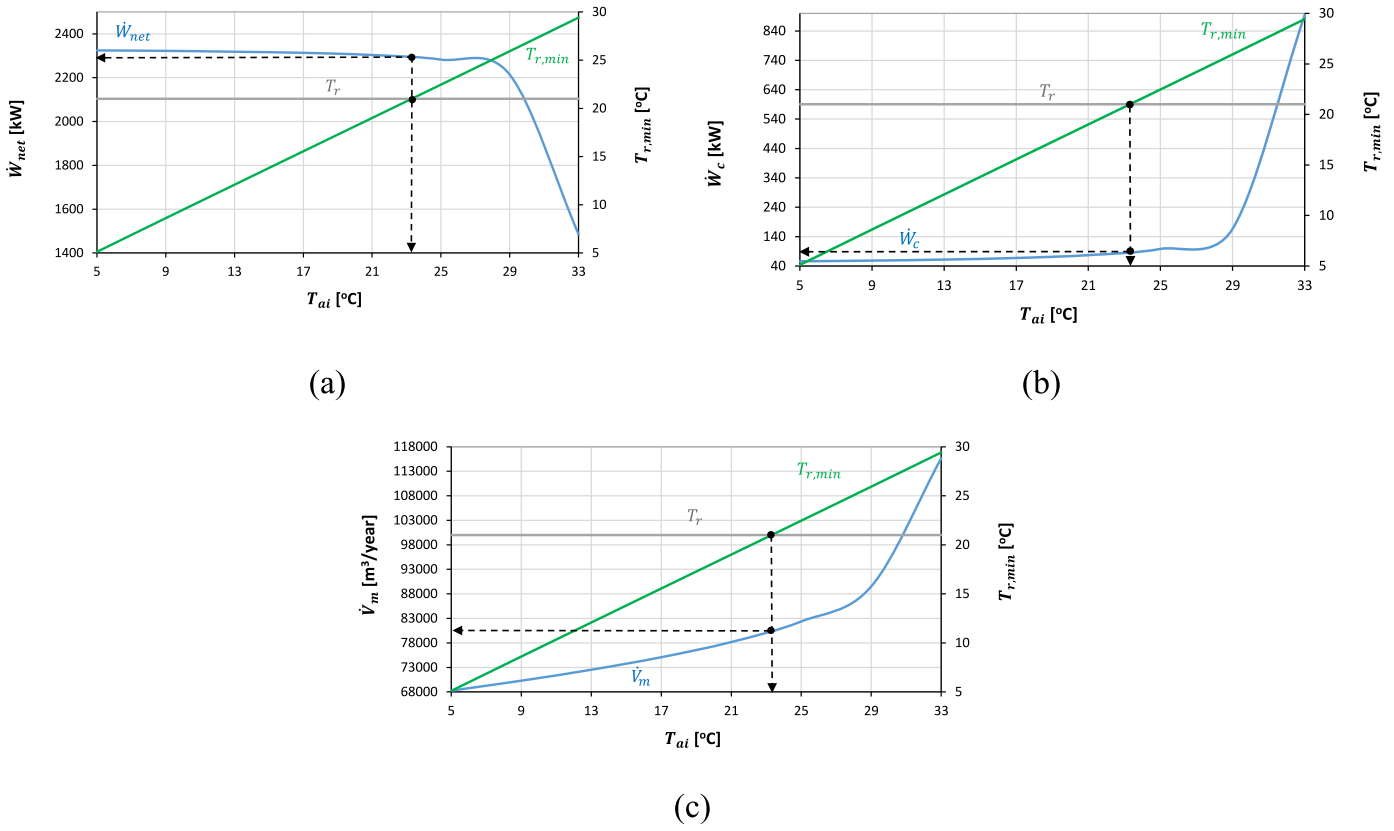

Fig. 25. Cooling temperature and (a) net mechanical power production, (b) mechanical power consumption, (c) thermal power production for DH vs. ambient temperature for the RRC.

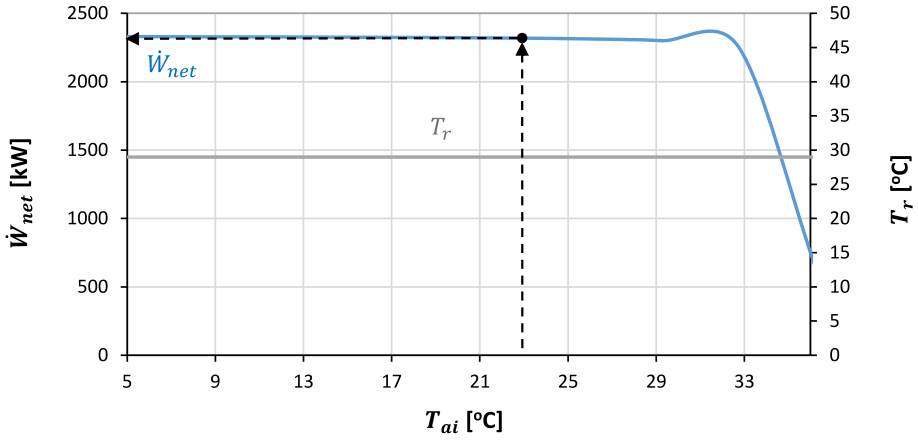

Fig. 26. Cooling temperature and net mechanical power production vs. ambient temperature for the base case of HCT.

specifications of the actual power plant under different operating conditions. A base case of both cycles was defined and compared, and several sensitivity analyses of the main variables were performed. T-s and Sankey diagrams of the base cases have also been presented to quantify the thermodynamic properties and energy distribution of the cycles. The HCT has been compared with the RRC keeping constant the condensation pressure at 0.078 bar, a thermal power supplied to the cycle of 10 MW and other operating parameters (steam pressure at the outlet of the steam generator, maximum temperature of the cycle, relative humidity of the environment, etc.). The results of the base case comparison show that the net power production of the HCT is 0.58 % higher than that of the RRC due to the lower total mechanical power consumption of pumps and fans (mainly in the dry coolers compared to the cooling tower). In addition, the thermal output for DH of the HCT is 1.59 % greater than that of the RRC.

Sankey diagrams show that the thermal power of the flows is greater in the HCT because of its layout and the condensation by absorption in the absorber. As a result, the thermal heat rejection of the HCT takes place under better conditions than in the RRC, avoiding the use of cooling towers and water consumption.

The effect of varying the bleeding mass flow to meet different DH requirements has also been studied. The net mechanical power decreases as the bleeding flow rate increases, and the net power provided by the HCT can be up to 0.7 % higher than that of the RRC under the same conditions. The thermal power for DH increases as the bleeding mass flow rate increases, and the influence of bleeding is stronger in the

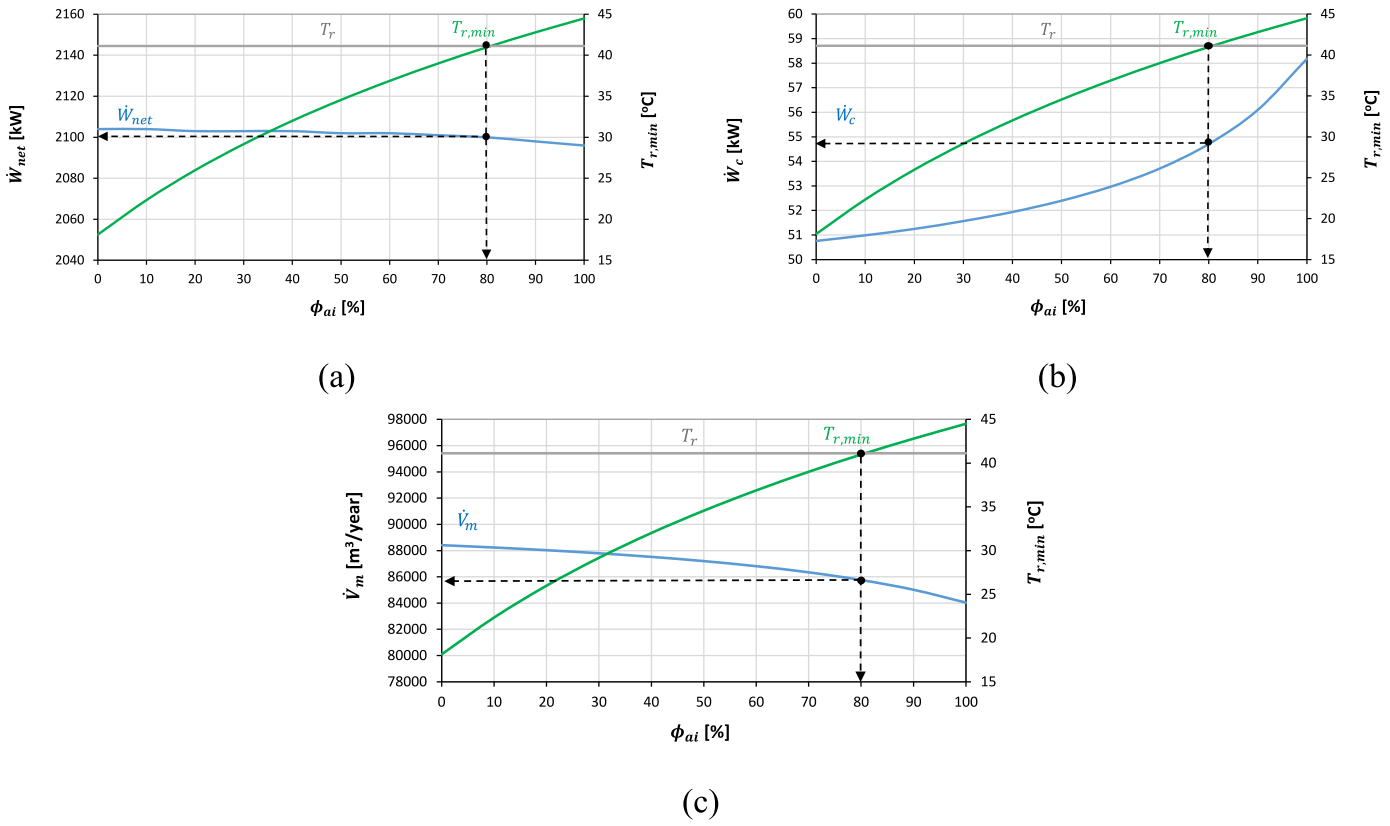

Fig. 27. Cooling temperature and (a) net mechanical power production, (b) mechanical power consumption, (c) thermal power production for DH vs. relative humidity of the ambient for the RRC at maximum condensing pressure.

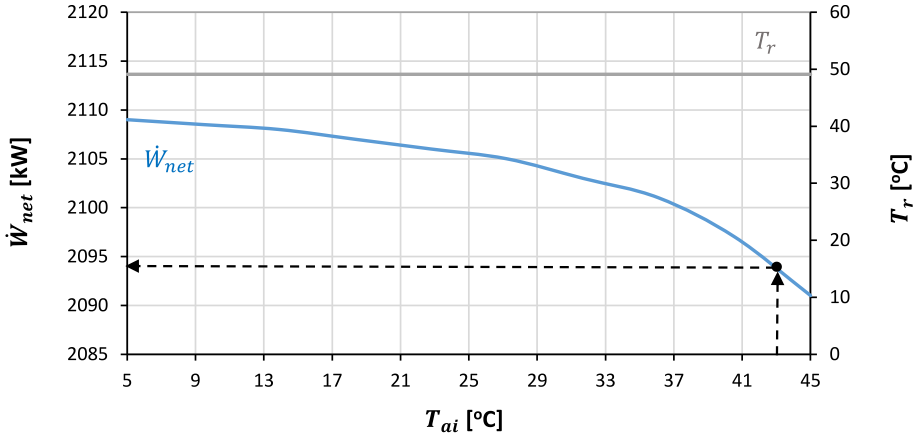

Fig. 28. Cooling temperature and net mechanical power production vs. ambient temperature for the HCT at the maximum condensing pressure.

HCT. The thermal power for DH can be 2.5 % higher for HCT than for RRC under the same operating conditions.

Considering 8000 h of plant operation per year, the cooling water consumption in the cooling tower of the RRC ranges from 70683.4 to 83842.6 m^3/year for the base case but varying the bleeding flow rate with the other conditions of the base case fixed. Therefore, with the implementation of the HCT, a significant amount of water can be saved in addition to improving the energy cycle performance.

Finally, sensitivity analyses were performed on key parameters such as condensing pressure, bleeding mass flow rate, and ambient temperature and relative humidity.

For the different condensing pressures studied, the thermal power for DH of the HCT increases up to 2.5 % with respect to RRC. Also, the higher the bleeding rate, the lower the increase in thermal power. The decrease in consumption of fans and pumps of HCT with respect to RRC varies from 4.11 to 27.9 %, with the higher values for lower condensing pressures. The increase of net mechanical power production ranges from 0.1 to 1 % with respect to RRC. The maximum thermal production for DH and the maximum net mechanical power are 2762 kW and 2417 kW respectively with the HCT and the water consumption can be of 84656 m^3/year at the maximum condensing pressure (0.21 bar), decreasing when the condensing pressure is lowered.

The maximum ambient temperature has been calculated for the RRC (23.5 °C) to operate, fixing the other specifications of the base case. At this temperature there is a decrease in net power and an increase in water consumption of 3.8 % and 3.9 %, respectively, compared to 20 °C. For the base case data of the HCT, but varying the ambient temperature, the maximum tolerable value to guarantee the operation of the dry

cooler is 23 °C. At this ambient temperature, the net power decreases by 0.37 % with respect to that of the base case (20 °C).

Regarding the effect of relative humidity, the decrease in both net power and water consumption of RRC are 5.9 % and 2.75 % respectively for the maximum considered (80 %), with reference to the 60 % humidity of the base case. Therefore, the increase in relative humidity has a significant negative effect on energy production, but a moderate positive effect on water consumption for the RRC.

According to the results and considering all possible operating conditions, the maximum ambient temperature admissible for the plant with the RRC is 41.5 °C, and that temperature is 1.62 °C higher with the HCT. Consequently, the availability of the cycle is greater with HCT, and the water consumption savings can reach values greater than 88000 m^3/year.

In summary, bleeding mass flow rate and condensing pressure are the variables with the greatest influence on the net power and thermal power for DH production. On the other hand, ambient temperature and to a lesser extent, the humidity are the variables with the highest influence the water consumption. This study shows that the implementation of HCT to a nuclear power plant with a Small Modular Reactor of 10 MW_{th} makes it more efficient for energy production and can save between 70000 and 88000 m^3/year of water, depending on the operating conditions. Extrapolation of these results to the generation mix implies that HCT is a good solution for improving the energy production of nuclear power plants, saving significant amounts of cooling water, and contributing significantly to the energy transition and more sustainable energy production.

Declaration of competing interest

The authors declare that they have no known competing financial interests or personal relationships that could have appeared to influence the work reported in this paper.

Data availability

Only the data included in the manuscript are available.

Acknowledgments

This work has been supported by the project "Improvement of energy performance of the Hygroscopic Cycle for power production from the Agencia Estatal de Investigación, Ministerio de Ciencia e Innovación, Spain (ref. PID2019-108325RB-I00/AEI/10.13039/501100011033); and "Severo Ochoa" grant program for training in research and teaching of the Principality of Asturias – Spain (BP20-176). The authors also want to acknowledge the contribution of the Spanish company IMATECH (IMASA TECHNOLOGIES), owner of the Hygroscopic cycle pilot plant, as well as the support from the University Institute of Industrial Technology of Asturias (IUTA), financed by the City Council of Gijón, Spain.

References

[1] J. Baek, A panel cointegration analysis of CO2 emissions, nuclear energy and income in major nuclear generating countries, Appl. Energy 145 (2015) 133–138.
[2] M.R. Pelissari, S.S.M. Cañas, M.O. Barbosa, C.C.G. Tassinari, Decarbonizing coal-fired power plants: carbon capture and storage applied to a thermoelectric complex in Brazil, Results Eng. 19 (2023), 101249.
[3] L. Liu, Y. Zhao, D. Chang, J. Xie, Z. Ma, Q. Sun, et al., Prediction of short-term PV power output and uncertainty analysis, Appl. Energy 228 (2018) 700–711.
[4] W. Wang, B. Yuan, Q. Sun, R. Wennersten, Application of energy storage in integrated energy systems — a solution to fluctuation and uncertainty of renewable energy, J. Energy Storage 52 (2022), 104812.
[5] A. Al Naimat, D. Liang, Substantial gains of renewable energy adoption and implementation in Maan, Jordan: a critical review, Results Eng. 19 (2023), 101367.
[6] IAEA, PRIS – Home. Database, Available from: https://pris.iaea.org/PRIS/home.aspx [Last access November 2023].
[7] IAEA, PRIS - Reactor status reports - Operational & Long-Term Shutdown - By Type. Database, Available from: https://pris.iaea.org/PRIS/WorldStatistics/OperationalReactorsByType.aspx [Last access November 2023].
[8] B.K. Sovacool, A. Gilbert, D. Nugent, An international comparative assessment of construction cost overruns for electricity infrastructure, Energy Res. Social Sci. 3 (2014) 152–160.
[9] M.S. Islam, M.P. Nepal, M. Skitmore, G. Kabir, A knowledge-based expert system to assess power plant project cost overrun risks, Expert Syst. Appl. 136 (2019) 12–32.
[10] P. Eash-Gates, M.M. Klemun, G. Kavlak, J. McNerney, J. Buongiorno, J. E. Trancik, Sources of cost overrun in nuclear power plant construction call for a New approach to engineering design, Joule 4 (11) (2020) 2348–2373.
[11] D. Sesma Martín, M. del M. Rubio-Varas, Freshwater for cooling needs: a long-run approach to the nuclear water footprint in Spain, Ecol. Econ. 140 (2017) 146–156.
[12] A. Elkouk, Y. Pokhrel, Y. Satoh, L. Bouchaou, Implications of changes in climate and human development on 21st-century global drought risk, J. Environ. Manag. 317 (2022), 115378.
[13] Z.M. El-Fakharany, M.G. Salem, Mitigating climate change impacts on irrigation water shortage using brackish groundwater and solar energy, Energy Rep. 7 (2021) 608–621.
[14] M.E. Malerba, N. Wright, P.I. Macreadie, Australian farm dams are becoming less reliable water sources under climate change, Sci. Total Environ. 829 (2022), 154360.
[15] S. Dehghani, A.R. Massah Bavani, A. Roozbahani, A. Gohari, R. Berndtsson, Towards an integrated system modeling of water scarcity with projected changes in climate and socioeconomic conditions, Sustain. Prod. Consum. 33 (2022) 543–556.
[16] D.J. Rodriguez, A. Delgado, P. DeLaquil, A. Sohns, Thirsty Energy, World Bank, Washington, DC, 2013. https://openknowledge.worldbank.org/handle/10986/16536. Last access November 2023.
[17] S.S. Ho, A.D. Leong, J. Looi, L. Chen, N. Pang, E. Tandoc Jr., Science literacy or value predisposition? A meta-analysis of factors predicting public perceptions of benefits, risks, and acceptance of nuclear energy, Environmental Communication 13 (4) (2019) 457–471.
[18] Y. Kim, W. Kim, M. Kim, An international comparative analysis of public acceptance of nuclear energy, Energy Pol. 66 (2014) 475–483.
[19] A. Harjanne, J.M. Korhonen, Abandoning the concept of renewable energy, Energy Pol. 127 (2019) 330–340.
[20] IPCC, Global warming of 1.5°C. An IPCC Special Report on the impacts of global warming of 1.5°C above pre-industrial levels and related global greenhouse gas emission pathways, in: P. Zhai, H.O. Portner, D. Roberts, J. Skea, P.R. Shukla, A. Pirani, W. Moufouma-Okia, C. Pean, R. Pidcock, S. Connors, J.B.R. Matthews, Y. Chen, X. Zhou, M.I. Gomis, E. Lonnoy, T. Maycock, M. Tignor, T. Waterfield (Eds.), The Context of Strengthening the Global Response to the Threat of Climate Change, Sustainable Development, and Efforts to Eradicate Poverty [V. Masson-Delmotte, World Meteorological Organization, Geneva, Switzerland, 2018. Summary for Policymakers.
[21] T. Bruckner, I.A. Bashmakov, Y. Mulugetta, H. Chum, A. de la Vega Navarro, J. Edmonds, A. Faaij, B. Fungtammasan, A. Garg, E. Hertwich, D. Honnery, D. Infield, M. Kainuma, S. Khennas, S. Kim, H.B. Nimir, K. Riahi, N. Strachan, R. Wiser, X. Zhang, Energy systems, in: O. Edenhofer, R. Pichs-Madruga, Y. Sokona, E. Farahani, S. Kadner, K. Seyboth, A. Adler, I. Baum, S. Brunner, P. Eickemeier, B. Kriemann, J. Savolainen, S. Schlomer, C. von Stechow, T. Zwickel, J.C. Minx (Eds.), Climate Change 2014: Mitigation of Climate Change. Contribution of Working Group III to the Fifth Assessment Report of the Intergovernmental Panel on Climate Change, Cambridge University Press, Cambridge, United Kingdom and New York, NY, USA, 2014.
[22] S.Y. Alhammadi, A.A. Alktebi, A.E. Eldemiery, V. Gillette, M.E.H. Assad, M. AlShabi, B.A. Khuwaileh, An extended thermosyphon cooling system for APR-1400 reactor design, Case Stud. Therm. Eng. 25 (2021), 100894.
[23] X. Yue, M.Y.P. Peng, M.K. Anser, A.A. Nassani, M. Haffar, K. Zaman, The role of carbon taxes, clean fuels, and renewable energy in promoting sustainable development: how green is nuclear energy? Renew. Energy 193 (2022) 167–178.
[24] V. Pershukov, V. Artisyuk, A. Kashirsky, Paving the way to green status for nuclear power, Sustainability 14 (15) (2022) 9339.
[25] The European Parliament and the Council of the European Union, Regulation (EU) 2020/852 of the European Parliament and of the Council of 18 June 2020 on the Establishment of a Framework to Facilitate Sustainable Investment, and Amending Regulation (EU) 2019/2088 (Text with EEA Relevance), 2020.
[26] Directorate-General for Financial Stability, Financial Services and Capital Markets Union, EU Taxonomy: Complementary Climate Delegated Act to Accelerate Decarbonisation, 2022.
[27] S. Hirschberg, C. Bauer, P. Burgherr, E. Cazzoli, T. Heck, M. Spada, K. Treyer, Health effects of technologies for power generation: contributions from normal operation, severe accidents and terrorist threat, Reliab. Eng. Syst. Saf. 145 (2016) 373–387.
[28] V.K.M. Cheng, G.P. Hammond, Life-cycle energy densities and land-take requirements of various power generators: a UK perspective, J. Energy Inst. 90 (2) (2017) 201–213.
[29] B.W. Brook, C.J. Bradshaw, Key role for nuclear energy in global biodiversity conservation, Conserv. Biol. 29 (3) (2014) 702–712.
[30] A. Peakman, Z. Hodgson, B. Merk, Advanced micro-reactor concepts, Prog. Nucl. Energy 107 (2018) 61–70.
[31] E.M.A. Hussein, Emerging small modular nuclear power reactors: a critical review, Physics Open 5 (2020), 100038.

[32] M.K. Rowinski, T.J. White, J. Zhao, Small and Medium sized Reactors (SMR): a review of technology, Renew. Sustain. Energy Rev. 44 (2015) 643–656.
[33] R. Testoni, A. Bersano, S. Segantin, Review of nuclear microreactors: status, potentialities and challenges, Prog. Nucl. Energy 138 (2021), 103822.
[34] S. Prasad, A. Abdulla, M.G. Morgan, I.L. Azevedo, Nonproliferation improvements and challenges presented by small modular reactors, Prog. Nucl. Energy 80 (2015) 102–109.
[35] Z. Liu, J. Fan, Technology readiness assessment of small modular reactor (SMR) designs, Prog. Nucl. Energy 70 (2014) 20–28.
[36] IAEA, Advances in Small Modular Reactor Technology Developments. A Supplement to: IAEA Advanced Reactor Information System (ARIS) 2020 Edition, International Atomic Energy Agency, 2020. https://aris.iaea.org/Publications/SMR_Book_2020.pdf [Last access November 2023.
[37] IAEA, ARIS - Technical Data. Database, Available from: https://aris.iaea.org/sites/SMR.html [Last access November 2023].
[38] D.T. Ingersoll, Z.J. Houghton, R. Bromm, C. Desportes, NuScale small modular reactor for Co-generation of electricity and water, Desalination 340 (2014) 84–93, 2014 May 1.
[39] S.T. Revankar, Chapter four - nuclear hydrogen production, in: H. Bindra, S. Revankar (Eds.), Storage and Hybridization of Nuclear Energy, Academic Press, 2019, pp. 49–117. https://www.sciencedirect.com/science/article/pii/B9780128139752000041. Last access November 2023.
[40] G. Locatelli, A. Fiordaliso, S. Boarin, M.E. Ricotti, Cogeneration: an option to facilitate load following in Small Modular Reactors, Prog. Nucl. Energy 97 (2014) 153–161, 2017 May 1.
[41] P.A. Wrigley, P. Wood, S. O'Neill, R. Hall, D. Robertson, Off-site modular construction and design in nuclear power: a systematic literature review, Prog. Nucl. Energy 134 (2021), 103664, 2021 Apr 1.
[42] S.M. Kissick, H. Wang, A comparative study of alternative power cycles for small modular reactors, Energy Convers. Manag. 247 (2021), 114734, 2021 Nov 1.
[43] N.P. Junior, J.R. Gazoli, A. Sete, R.M. Velasquez, J.D. Hunt, F.T. Bindemann, K.A. R. Ismail, Climate impact on combined cycle thermoelectric power plant in hot and humid regions, Results Eng. 19 (2023), 101342.
[44] N. Petchers, Combined Heating, Cooling & Power Handbook: Technologies & Applications an Integrated Approach to Energy Resource Optimization, The Fairmont Press Distributed by Marcel Dekker, Lilburn, GA New York, NY, 2012.
[45] Y.A. Cengel, M.A. Boles, M. Kanoğlu, Thermodynamics: an Engineering Approach, vol. 5, McGraw-hill, New York, 2011, p. 445.
[46] A. Tiktas, H. Gunerhan, Hepbasli, A. Single and multigeneration Rankine cycles with aspects of thermodynamical modeling, energy and exergy analyses and optimization: a key review along with novel system description figures, Energy Convers. Manag. X 14 (2022), 100199, 2022 May 1.
[47] T. Wang, Y. Zhang, Z. Peng, G. Shu, A review of researches on thermal exhaust heat recovery with Rankine cycle, Renew. Sustain. Energy Rev. 15 (6) (2011) 2862–2871, 2011 Aug 1.
[48] K. Rahbar, S. Mahmoud, R.K. Al-Dadah, N. Moazami, S.A. Mirhadizadeh, Review of organic Rankine cycle for small-scale applications, Energy Convers. Manag. 134 (2017) 135–155, 2017 Feb 15.
[49] J. Li, X. Peng, Z. Yang, S. Hu, Y. Duan, Design, improvements and applications of dual-pressure evaporation organic Rankine cycles: a review, Appl. Energy 311 (2022), 118609, 2022 Apr 1.
[50] A. Kasaeian, A. Shamaeizadeh, B. Jamjoo, Combinations of Rankine with ejector refrigeration cycles: recent progresses and outlook, Appl. Therm. Eng. 211 (2022), 118382, 2022 Jul 5.
[51] Cooling of Power Plants - World Nuclear Association. Available from: https://world-nuclear.org/our-association/publications/technical-positions/cooling-of-power-plants.aspx. [Last access November 2023].
[52] A. Chesi, L. Ferrari, G. Ferrara, E.A. Carnevale, Feasibility of small-size biomass-fueled hirn-cycle cogeneration plants, Energy Proc. 81 (2015) 155–164.
[53] L.M. Romeo, S. Espatolero, I. Bolea, Designing a supercritical steam cycle to integrate the energy requirements of CO2 amine scrubbing, Int. J. Greenh. Gas Control 2 (4) (2008) 563–570.
[54] A. Meana-Fernández, B. Peris-Pérez, A.J. Gutiérrez-Trashorras, S. Rodríguez-Artime, J.C. Ríos-Fernández, J.M. González-Caballín, Optimization of the propulsion plant of a Liquefied Natural Gas transport ship, Energy Convers. Manag. 224 (2020), 113398.
[55] I. Dincer, H. Al-Muslim, Thermodynamic analysis of reheat cycle steam power plants, Int. J. Energy Res. 25 (8) (2001) 727–739.
[56] Y. Ying, E.J. Hu, Thermodynamic advantages of using solar energy in the regenerative Rankine power plant, Appl. Therm. Eng. 19 (11) (1999) 1173–1180.
[57] S. Subbiah, R. Natarajan, Thermodynamic analysis of binary-fluid Rankine cycles for geothermal power plants, Energy Convers. Manag. 28 (1) (1988) 47–52.
[58] J.P. Njock, M.N. Ngangué, O.T. Sosso, R. Nzengwa, Highlighting the effect of the lower operating limit of the condenser on ORC working fluids selection, Results Eng. 19 (2023), 101369.
[59] S.S. Bishal, D.F. Faysal, M.M. Ehsan, S. Salehin, Performance evaluation of an integrated cooling and power system combining supercritical CO2, gas turbine, absorption refrigeration, and organic Rankine cycles for waste energy recuperating system, Results Eng. 17 (2023), 100943.
[60] K.J. DiGenova, B.B. Botros, J.G. Brisson, Method for customizing an organic Rankine cycle to a complex heat source for efficient energy conversion, demonstrated on a Fischer Tropsch plant, Appl. Energy 102 (2013) 746–754.
[61] B. Peris, J. Navarro-Esbrí, C. Mateu-Royo, A. Mota-Babiloni, F. Molés, A. J. Gutiérrez-Trashorras, M. Amat-Albuixech, Thermo-economic optimization of small-scale organic Rankine cycle: a case study for low-grade industrial waste heat recovery, Energy 213 (2020), 118898.
[62] N.P. Chaimongkol, T. Thoranis Deethayat, D. Wang, T. Kiatsiriroat, Waste heat harvesting from continuous blowdown for power generation via organic Rankine cycle network: case study of a coal-fired power plant, Results Eng. 20 (2023), 101543.
[63] T.D. Agonafer, W.B. Eremed, K.D. Adem, Biogas-based trigeneration system: a review, Results Eng. (2022), 100509.
[64] F. Raab, H. Klein, F. Opferkuch, Steam Rankine cycle instead of organic Rankine cycle for distributed high temperature waste heat recovery – pros and cons, in: Proceedings of the 6th International Seminar on ORC Power Systems, Technical University of Munich: Technical University of Munich, 2021.
[65] H.H. Zhang, M.J. Li, Y.Q. Feng, H. Xi, T.C. Hung, Assessment and working fluid comparison of steam Rankine cycle -Organic Rankine cycle combined system for severe cold territories, Case Stud. Therm. Eng. 28 (2021), 101601.
[66] H. Sayyaadi, T. Sabzaligol, Comprehensive exergetic and economic comparison of PWR and hybrid fossil fuel-PWR power plants, Energy 35 (7) (2010) 2953–2964.
[67] M. Kahraman, A.B. Olcay, E. Sorgüven, Thermodynamic and thermoeconomic analysis of a 21 MW binary type air-cooled geothermal power plant and determination of the effect of ambient temperature variation on the plant performance, Energy Convers. Manag. 192 (2019) 308–320.
[68] S. Pan, S.W. Snyder, A.I. Packman, Y.J. Lin, P. Chiang, Cooling water use in thermoelectric power generation and its associated challenges for addressing water-energy nexus, Water-Energy Nexus (2018) 26–41.
[69] J. Macknick, R. Newmark, G. Heath, K.C. Hallett, Operational water consumption and withdrawal factors for electricity generating technologies: a review of existing literature, Environ. Res. Lett. 7 (4) (2012), 045802, 2012 Dec.
[70] M. Yaqub, S.M. Zubair, Performance characteristics of counter flow wet cooling towers, Energy Convers. Manag. 44 (13) (2003) 2073–2091.
[71] E.S. Spang, W.R. Moomaw, K.S. Gallagher, P.H. Kirshen, D.H. Marks, The water consumption of energy production: an international comparison, Environ. Res. Lett. 9 (10) (2014), 105002.
[72] Ablimit Aili, et al., Reduction of water consumption in thermal power plants with radiative sky cooling, Appl. Energy 302 (2021), 117515.
[73] F.J. Rubio Serrano, F. Soto Pérez, A.J. Gutiérrez Trashorras, G. Ausin Abad, Comparison between existing rankine cycle refrigeration systems and hygroscopic cycle technology, in: International Research Conference on Sustainable Energy, Engineering, Materials and Environment, 2018, pp. 25–27 (Mieres, Asturias, Spain).
[74] F.J. Rubio-Serrano, F. Soto-Pérez, A.J. Gutiérrez-Trashorras, Experimental study on the influence of the saline concentration in the electrical performance of a Hygroscopic cycle, Appl. Therm. Eng. 165 (2020), 114588, 2020 Jan 25.
[75] A. Meana-Fernández, J.M. González-Caballín, R. Martínez-Pérez, F.J. Rubio-Serrano, A.J. Gutiérrez-Trashorras, Power plant cycles: evolution towards more sustainable and environmentally friendly technologies, Energies 15 (23) (2022) 8982.
[76] F.J. Rubio-Serrano, A.J. Gutiérrez-Trashorras, F. Soto-Pérez, E. Álvarez-Álvarez, E. Blanco-Marigorta, Advantages of incorporating Hygroscopic Cycle Technology to a 12.5-MW biomass power plant, Appl. Therm. Eng. 131 (2018) 320–327, 2018 Feb 25.
[77] F.J. Rubio-Serrano, F. Soto-Pérez, A.J. Gutiérrez-Trashorras, Influence of cooling temperature increase in a hygroscopic cycle on the performance of the cooling equipment, Energy Convers. Manag. 200 (2019), 112080.
[78] F.J. Rubio-Serrano, R. Martínez-Pérez, A. Meana-Fernández, J.M. González-Caballín, A.J. Gutiérrez-Trashorras, Experimental study on the influence of electrical conductivity of hygroscopic compounds on the performance of a hygroscopic cycle, Appl. Therm. Eng. 233 (2023), 121181.
[79] M. Potesta-González, R. Martínez-Pérez, A. Meana-Fernández, F.J. Rubio-Serrano, A.J. Gutiérrez-Trashorras, Analytical study for the comparison between hygroscopic and Rankine cycle. An exergy approach, Energy Convers. Manag. 292 (2023), 117394.
[80] Martínez-Pérez, R., Meana-Fernández, A., González-Caballín, J. M., Manfredi, A., Rubio-Serrano, F. J., & Gutiérrez-Trashorras, A. J. Analytical study of the waste heat in a Hygroscopic Cycle with high lithium bromide concentration for energy use. Proceedings of ECOS 2023 - the 36th International Conference on Efficiency, Cost, Optimization, Simulation and Environmental Impact of Energy Systems 25-30 June 2023, (Las Palmas De Gran Canaria, Spain).
[81] R. Martínez-Pérez, B. Peris-Pérez, J.C. Ríos-Fernández, J.M. González-Caballín, F. Rubio-Serrano, A.J.G. Trashorras, Analytical model of the refrigeration system for cooling in a hygroscopic cycle power plant, in: 21th International Conference on Renewable Energies and Power Quality (ICREPQ'23). Madrid (Spain), 2023, 24th to 26th May.
[82] M. Potesta-González, R. Martínez-Pérez, A. Meana-Fernández, J.M. González-Caballín Sánchez, F.J. Rubio-Serrano, A.J. Gutiérrez-Trashorras, Analytical study of the absorber performance of a Hygroscopic cycle for low concentrations of LiBr solutions, in: 21th International Conference on Renewable Energies and Power Quality (ICREPQ'23), 2023. Madrid (Spain), 24th to 26th May.
[83] J.C. Ríos-Fernández, R. Martínez-Pérez, V.M. Fernández-Pacheco, A. Meana-Fernández, F.J. Rubio-Serrano, A.J. Gutiérrez-Trashorras, Water saving in electric power generation facilities using the hygroscopic cycle in the subtropical climate, in: Proceedings of ECOS 2023 - the 36th International Conference on Efficiency, Cost, Optimization, Simulation and Environmental Impact of Energy Systems 25-30 June, Las Palmas De Gran Canaria, Spain, 2023.
[84] M.A. Alzamly, M. Aziz, A.A. Badawi, H.A. Gabal, A.R.A. Gadallah, Burnup analysis for HTR-10 reactor core loaded with uranium and thorium oxide, Nucl. Eng. Technol. 52 (4) (2020) 674–680, 2020 Apr 1.
[85] IAEA, Evaluation of High Temperature Gas Cooled Reactor Performance: Benchmark Analysis Relate to Initial Testing of the HTTR and HTR-10 (Part 2 -

Chapter 4), IAEA, Viena, Austria, 2003. Available from: https://www-pub.iaea.org/MTCD/publications/PDF/te_1382_web/TE_1382_Part2.pdf. Last access November 2023.
[86] F-Chart Software, EES Engineering Equation Software. https://www.fchartsoftware.com/ees/. [Last access November 2023].
[87] Y.O. Devres, Psychrometric properties of humid air: calculation procedures, Appl. Energy 48 (1) (1994) 1–18.
[88] IDAE. Technical guide of cooling towers. Institute for Energy Diversification and Saving. Madrid. Spain. https://www.idae.es/uploads/documentos/documentos_10540_Torres_refrigeracion_GT4_07_05eca613.pdf. [Last access November 2023].
[89] S. Mohtaram, Y. Sun, M. Omidi, J. Lin, Energy-exergy efficiencies analyses of a waste-to-power generation system combined with an ammonia-water dilution Rankine cycle, Case Stud. Therm. Eng. 25 (2021), 100909, 2021.
[90] G. Fan, Y. Gao, H. Ayed, R. Marzouki, Y. Aryanfar, F. Jarad, P. Guo, Energy and exergy and economic (3E) analysis of a two-stage organic Rankine cycle for single flash geothermal power plant exhaust exergy recovery, Case Stud. Therm. Eng. 28 (2021), 101554, 2021.
[91] A. Nemati, H. Nami, F. Ranjbar, M. Yari, A comparative thermodynamic analysis of ORC and Kalina cycles for waste heat recovery: a case study for CGAM cogeneration system, Case Stud. Therm. Eng. 9 (2017) 1–13.
[92] R.K. Kapooria, S. Kumar, K.S. Kasana, An analysis of a thermal power plant working on a Rankine cycle: a theoretical investigation, J. Energy South Afr. 19 (1) (2008) 77–83.
[93] M.J. Moran, H.N. Shapiro, D.D. Boettner, M.B. Bailey, Fundamentals of Engineering Thermodynamics, John Wiley & Sons, 2010.
[94] M.A. Habib, S.M. Zubair, Second-law-based thermodynamic analysis of regenerative-reheat Rankine-cycle power plants, Energy 17 (3) (1992) 295–301.
[95] M.O. Karaağaç, A. Kabul, H. Oğul, First-and second-law thermodynamic analyses of a combined natural gas cycle power plant: Sankey and Grossman diagrams, Turk. J. Phys. 43 (1) (2019) 93–108.
[96] T. Yamamoto, T. Furuhata, N. Arai, K. Mori, Design and testing of the organic Rankine cycle, Energy 26 (3) (2001) 239–251.
[97] M.M. Rashidi, N. Galanis, F. Nazari, A.B. Parsa, L. Shamekhi, Parametric analysis and optimization of regenerative Clausius and organic Rankine cycles with two feedwater heaters using artificial bees colony and artificial neural network, Energy 36 (9) (2011) 5728–5740.
[98] J.C. Hensley (Ed.), Cooling Tower Fundamentals, Marley Cooling Tower Company, Stockton, CA, 1985.
[99] C. Schulze, B. Raabe, C. Herrmann, S. Thiede, Environmental impacts of cooling tower operations–The influence of regional conditions on energy and water demands, Procedia CIRP 69 (2018) 277–282.
[100] N. Milosavljevic, P. Heikkilä, A comprehensive approach to cooling tower design, Appl. Therm. Eng. 21 (9) (2001) 899–915.